INDERSCIENCE PUBLISHERS
Linking academia, business and industry through research

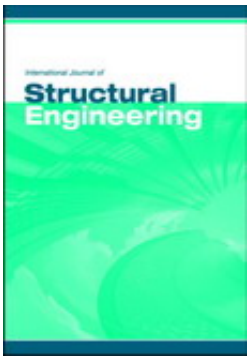

International Journal of Structural Engineering

ISSN online: 1758-7336 - ISSN print: 1758-7328
https://www.inderscience.com/ijstructe

A review on fabrication and dynamic characterisation of composite beam structure

J. Akshobya, Mantesh Basappa Khot

DOI: 10.1504/IJSTRUCTE.2022.10047780

Article History:
Received: 11 February 2022
Accepted: 23 March 2022
Published online: 07 November 2022

A review on fabrication and dynamic characterisation of composite beam structure

J. Akshobya and Mantesh Basappa Khot*

Department of Mechanical Engineering,
PES University,
Bangalore-560085, Karnataka, India
Email: akshobya997@gmail.com
Email: mahanteshbk@pes.edu
*Corresponding author

Abstract: This review article focused to highlight the recent studies conducted to explore the dynamics characteristics of fibre-reinforced composite via. experimental and numerical approaches for different volume ratios analysed for various boundary conditions. Because of the benefits in performance, structural efficiency, and cost that improved composite materials give, they are progressively being used in aircraft, marine, and other industries. The vibration effect in most of the applications is unpleasant causing user discomfort, noise, bodily health problems, and structural endurance problems. It is necessary to understand dynamic characteristics viz., natural frequencies (ω_n), damping characteristics (C), and frequency response function (FRF) of the beam. This article focused on various fabrication technologies utilised in the manufacturing of aramid fibre composite beams. Based on the available literature polymerisation induced self-assembly fabrication technique used to produce the aramid fibre and FFT analyser is widely used to analyse the dynamic characteristics of the beam structure.

Keywords: aramid fibre; natural frequencies; damping characteristics; frequency response function; FRF.

Reference to this paper should be made as follows: Akshobya, J. and Khot, M.B. (2023) 'A review on fabrication and dynamic characterisation of composite beam structure', *Int. J. Structural Engineering*, Vol. 13, No. 1, pp.22–62.

Biographical notes: J. Akshobya received his BE degree in Mechanical Engineering from the B.N.M. Institute of Technology afflicted to Visvesvaraya Technological University and currently pursing MTech in Machine Design from the PES University Bangalore. His research interests are in the area of dynamic characteristics of materials and composite material characterisation using experimental tests.

Mantesh Basappa Khot received his BE degree in Mechanical Engineering from University BDT College of Engineering, Davangere, and have done MTech in machine design from University BDT College of Engineering, Davangere. His research interest are fracture and fatigue analysis of materials, mechanics of composite materials, vibrational characteristics of materials, characterisation of composite materials and design of experiments. Currently, he is working as an Assistant Professor in Design Domain at Mechanical Engineering Department, PES University Bangalore till date.

1 Introduction

A composite is a blend of two or more elements that can be combined in any way and for a range of purposes. The idea behind composite materials is that mixing multiple elements often results in a new material that performs better than its separate constituents. Composite materials applications have developed gradually over time, infiltrating and conquering more markets in the process. Composites are preferred because of their outstanding strength-to-weight ratios, long fatigue life, high stiffness, and other material features, composite beams have become extremely popular in a variety of forms of industrial applications in the previous couple of decades. These engineered material industries, which range from everyday goods to sophisticated technical applications, are dominated by modern and established composite materials. Construction, military, automobile, and aerospace industries all used these sophisticated materials. Their technologies are particularly appealing since they outperform most existing materials, such as metal, in terms of specific strength, density, lightweight, corrosion resistance, and temperature capacity (Ishak et al., 2013). High aspect ratio, high porosity, large specific surface area, and unique nanotechnology effects describe polymer fibre and its derivatives, making them potential building blocks in a variety of developing applications (Huang et al., 2004; Deitzel et al., 2001; Pham et al., 2006).

Yang et al. in 2011 initially created aramid nanofibre (ANF), a 1D nanofibre with great strength and modulus, a large specific surface area, a high aspect ratio, and excellent chemical stability and thermal by substantial efficiency macroscopic poly(p-phenylene terephthalamide) (PPTA) fibre. Since 2011, year after year, the number of publications and citations about ANF has increased especially in the previous three years, as seen in Figure 1(a). Furthermore, as shown in Figure 1(b), there have been studies on ANF in a variety of disciplines, including materials science, engineering, chemistry, and polymer science, demonstrating the growing interest in ANF from a variety of sources. It's a promising nanoscale building block that's been used in a variety of composite reinforcing applications (Yang et al., 2015; Nasser et al., 2019; Fan et al., 2012).

Figure 1 Annual ANF publications and citations as reported by ISI Web of Science, (a) numbers of publications and citations every year (b) the distribution of citing papers across various fields of study (see online version for colours)

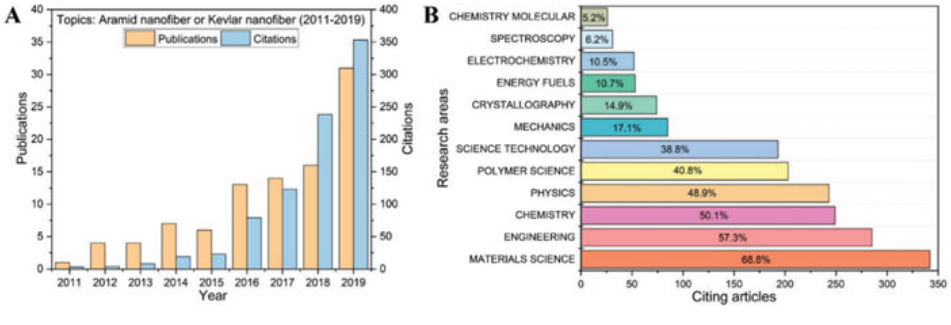

Source: Yang et al. (2020)

The top-down method is used to make ANF from macroscopic PPTA fibre. DuPont invented PPTA fibre in the 1960s, which is also Kevlar and Twaron by two commercial names for the same material (Yang et al., 2020).

Figure 2 PPTA fibre preparation and structural characteristics, (a) Diagram of the manufacturing pro (b) photographs of PPTA separated fibres [with permission, this image has been reproduced (Teijin, 2019)] (c) PPTA fibre SEM picture [with permission, this image has been reproduced (Yang et al., 2019a)] (d) illustration of the PPTA molecular structure, demonstrating the strong intermolecular interactions in the radial direction that cause hydrogen-bonded sheets to stack [with permission, this image has been reproduced (DuPont, 2019)] (see online version for colours)

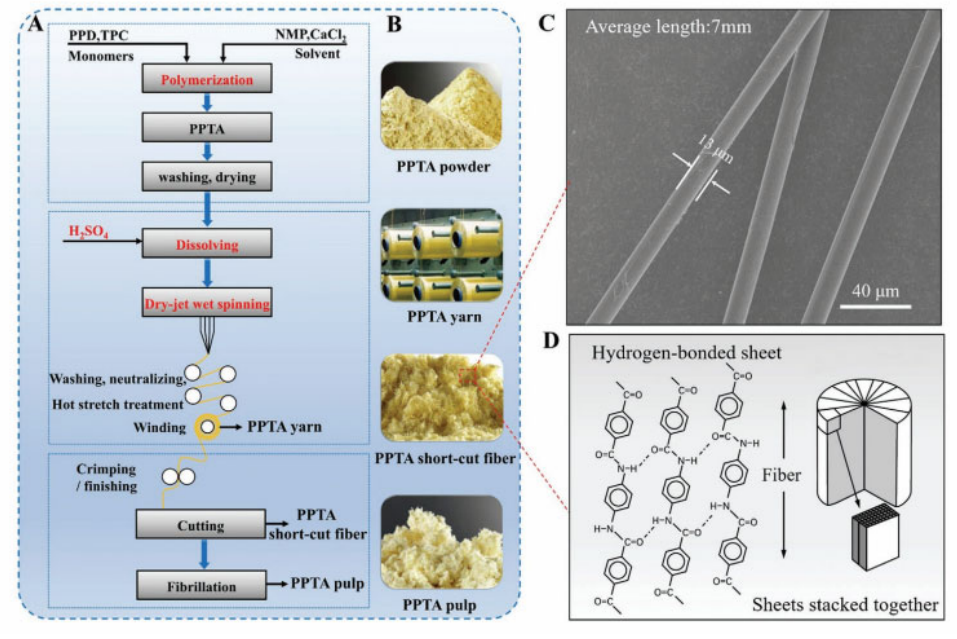

Figure 2(a) shows how PPTA fibre is made from PPTA/H_2SO_4 liquid crystals after polymerisation of terephthaloyl chloride and p-phenylenediamine in an N-methyl-pyrrolidone/$CaCl_2$ system using a dry-jet wet spinning approach (Yang et al., 2017). Figure 2(b) shows how PPTA fibre after spinning, is post-treated to produce distinct PPTA fibres with diverse morphologies for different purposes, such as PPTA pulp, short-cut fibre, and PPTA yarn. As illustrated in Figure 2(c), PPTA fibre has a flat surface and no active functional groupings, resulting in poor interfacial interaction between the polymer matrix and PPTA fibre. Because of its stiff molecular chains and high crystallinity, PPTA fibre, as one of three high-tech polymeric fibres, has outstanding mechanical capabilities, chemical inertness, and excellent thermal stability as shown in Figure 2D (Rao et al., 2001; Roenbeck et al., 2019; Grujicic et al., 2013; Cheng et al., 2005).

2 Preparation and fabrication methods of ANFs and composite respectively

Due to its regular molecular chain structure and hydrogen connections between molecular chains, aramid fibres combine great mechanical capabilities, chemical stability, thermal stability, low density, and pose many obstacles in the research of ANFs. In 2011, Yang et al. were the first to disclose the production of ANFs from an alkaline DMSO solution. Aramid fibre must be pre-treated and then post-treated in all three approaches. The four basic ways of making ANFs are top-down electrospinning, deprotonation, bottom-up, and mechanical breakdown polymerisation. It is crucial to note that, whereas the published articles have gone into great detail about ANF preparation methods, the current review only presents a quick overview of the combination of ANF and epoxy resin composite.

2.1 Electrospinning

'Electrospinning' comes from the term 'electrostatic spinning'. A high-voltage source, a capillary tube with a small needle, and a grounded collecting screen are required for the technique (Kulkarni et al., 2010; Yao et al., 2010). This process resulted in fibre with smaller diameters as well as excellent mechanical properties. This led to the formation of the electrospinning technology, which can create nanofibres with diameters ranging from 10 nm to 10 mm. (Park et al., 2007). Figure 3 shows a schematic representation, while Figure 4 shows a photographic view. A high voltage is required to produce a polymer solution jet from an electrically charged needle. The solution evaporates or solidifies before reaching the collector screen, and is collected as an interconnected web of fine fibres. The spinning solution is connected to one electrode, while the grounded collector is connected to the other. The solution fluid is maintained in place by surface tension and is held in place by an electric field delivered to the capillary tube's end. As the electrical field intensity increases, the hemispherical surface of the fluid at the capillary tube's tip elongates, generating a conic shape known as a 'Taylor cone' (Nirmala et al., 2014; Yang et al., 2019b).

Figure 3 The electrospinning process is depicted in a diagram

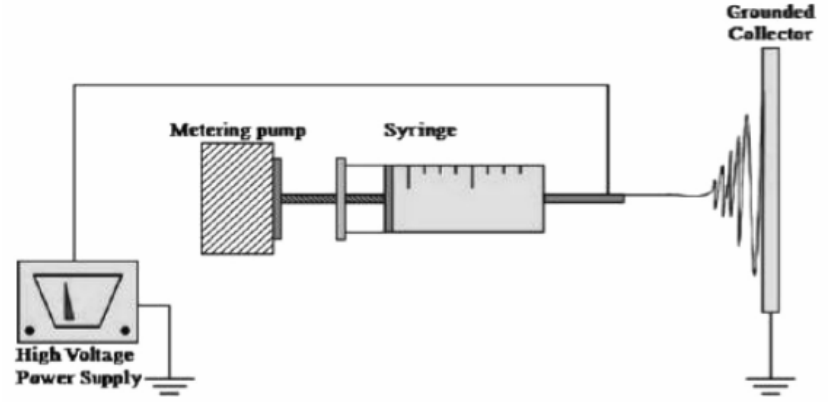

Source: Kulkarni et al. (2010)

The mechanical properties of the lowest diameter fibres in these branch PPTA fibres were much greater in aramid fibre produced by the electrospinning process, with Young's modulus and tensile strength values of 59 and 1.1 GPa for fibres with a diameter of 2.1 mm, respectively. To forecast the properties of the fibres, a geometrical model based on a reduction for the size-dependent Young's modulus was investigated (Yao et al., 2015).

Figure 4 Photographic image of the electrospinning setup

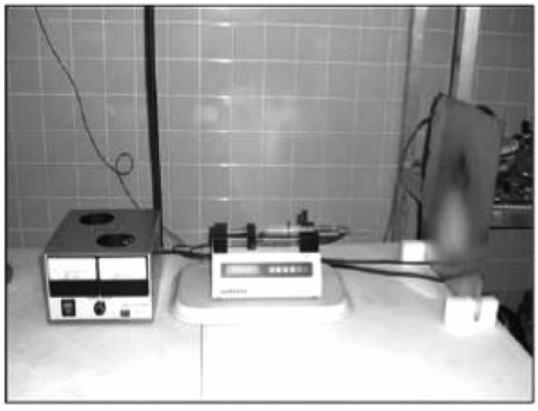

Source: Kulkarni et al. (2010)

2.2 Mechanically assisted preparation

The chemical structures of ANFs generated with mechanical help are usually not destroyed, and the original superior mechanical qualities, chemical stability, and high-temperature resistance of ANFs are maintained. Ifuku et al. (2014) by mechanically treating para-aramid fibres with NaOH, p-ANFs are created which contain para-crystallite. Using electrostatic repelling force, it was easy to divide into nanofibre with large effective mechanical and surface-to-volume ratio characteristics. After hot pressing at 100 °C, the average tensile strength, Young's modulus, and strain of P-ANFs sheets made by the filtering process are 2.0 GPa, 26.8 MPa, and 1.5%, respectively. The preparation method has a significant impact on these mechanical qualities. Lately, Gonzalez et al. (2017) have deliberate immersion rotary jet-spinning (IRJS) is a centrifugal force method for manufacturing nanofibre here the use of high voltage is avoided. P-ANFs with a diameter of 500–1000 nm were used in the study for effectively manufacturing using this approach and showed good mechanical properties. The practical applicability of this method, however, due to the use of sophisticated equipment and low manufacturing efficiency is severely limited.

2.3 Deprotonation and its improvement

Yang et al. (2011) deprotonation was originally reported in 2011 for the synthesis of an alkaline DMSO solution yielded ANFs with a diameter of 3–30 nm and a length of up to 10 m. The synthesised ANFs have promising thermal and mechanical properties, as well as a high aspect ratio, indicating that they could be used as a novel nanoscale building

block. The deprotonation process, unlike the other two, does not involve the purchase of heavy equipment or elaborate stages, and merely requires stirring at ambient temperature. Cao et al. (2013) investigated to make stable ANF dispersions, commercial para-aramid yarns were immersed in KOH-DMSO solutions. The ANFs were then hydrolysed using phosphoric acid (PA) and bent with glutaraldehyde (GA). Following that, the ANFs were vacuum-assisted filtered into macroscopic thin films. However, there are several drawbacks to fabricating deprotonation of ANFs has several drawbacks, including a lengthy method (about 7 days) and low preparation efficiency. Luo et al. (2019) the various ANFs and their films generated from conventional aramid woven, chopped fibre, and pulp fibre respectively, were examined. The ANFs films formed from chopped fibre had outstanding mechanical capabilities and thermal stability according to the data, the material has an ultimate strength of 103.41 MPa and stiffness of 4.70 GPa. Wu et al. (2019) described a simple vacuum-assisted suction approach for fabricating ANFs membranes generated by various proton donors (water or ethanol). Because ethanol is a poorer proton donor, the tensile strength of the ANFs membrane aided by water (203.92 MPa) is higher than that of the membrane supported by ethanol (141.34 MPa). Rapakousiou et al. (2020) presented a new approach for producing ANFs that involves employing oligo-(6-pyrene terephthalamide, oPyrTA) as an oligoamide model for Kevlar and then deprotonating the nanofibres. Although the deprotonation method has several advantages, such as mild reaction conditions, a lack of expensive equipment, and simple operating procedures, the method's long preparation cycle, and low preparation efficiency appears to be the main barriers to its industrial application.

2.4 Polymerisation induced self-assembly

To make ANFs, all three procedures require pre-treating aramid fibre and then post-treating aramid fibre, which is complicated, time-consuming, and inefficient. Yan et al. (2016) introduced a technique for using methoxy polyethylene glycol (mPEG) as an interfacial customising and dispersion agent. The presence of mPEG is required for the production of ANFs.

Figure 5 ANFs' molecular formula and surface shape are depicted. The ANFs have a high aspect ratio and excellent thermal stability, as well as improved water solubility in solvents like water or ethanol. Simple procedures no complicated equipment and great preparation efficiency for characteristics of the polymerisation induced self-assembly approach, making it perfect for mass production on a wide scale. There are numerous techniques for creating ANFs with various structures. Huang et al. (2013) created stiff, structural units of aromatic aramid molecules that can self-assemble into nanofibre spontaneously. In Yoshioka and Tashiro (2014) and Yoshioka (2012), aromatic polyamide nanofibres with trifluoromethyl (CF3) groups were prepared using a precipitation polymerisation approach using 4, 4-diphenyldicarbonyl chloride and 2, 2-bis (trifluoromethyl) benzidine in a dioxane solution including water. By altering the content of the reaction fluid, the morphology of the aromatic polyamide nanofibres may be changed dramatically. The aromatic polyamide nanofibres were found to have high thermal stability and chemical resistance as-prepared. Yoshioka (2017) then used an annealing procedure to evaluate the structural changes in aromatic polyamide nanofibre. Aromatic polyamide nanofibre' intermolecular hydrogen bonding and crystallinity increased after annealing, but their surface shape remained constant. These technologies produce nanofibre that is unsuitable for industrial applications.

Figure 5 (a) Surface morphology of ANFs (b) TEM (c) AFM (d) Molecular structures of ANFs; Tyndall effect of PPTA nanofibre colloid (see online version for colours)

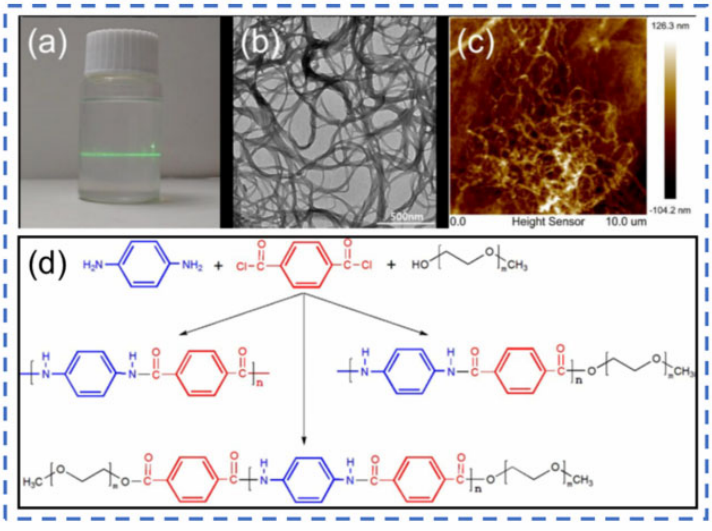

Source: Yan et al. (2016)

Table 1 The benefits and drawbacks of different ANF preparation approach

Preparation method	*Advantages*	*Disadvantages*	*Time (h)*
Electrospinning	• Continuous spinning	• Complicated steps • Corrosion equipment • High cost	• ~24
Mechanical disintegration	• Excellent performance	• High energy consumption • Requirements for equipment	• ~24
Deprotonation	• Simple steps • Mild conditions	• Long preparation cycle • Low efficiency	• ~168
Polymerisation induced self-assembly	• No need of AMFs • Simple steps • High efficiency	• None	• N/A

As shown in Table 1, the advantages and disadvantages of various ANF preparation approaches were discussed. The polymerisation-induced self-assembly method can be used to avoid the formation of AMFs and is cost-effective, efficient, and simple to implement on a large scale. Furthermore, the ANFs as-prepared has excellent mechanical characteristics and water dispersibility, making them ideal for application in polymer reinforcement. The following sections look at how ANFs can improve the mechanical characteristics of a variety of polymers.

Figure 6 (a) Separated ANF reinforced epoxy nanocomposites with different weight fractions have different mechanical characteristics (Jung and Sodano, 2020) (b) Mechanical properties of modified with epoxy ANFs added to epoxy and mechanical characteristics comparison (Lin et al., 2017) (see online version for colours)

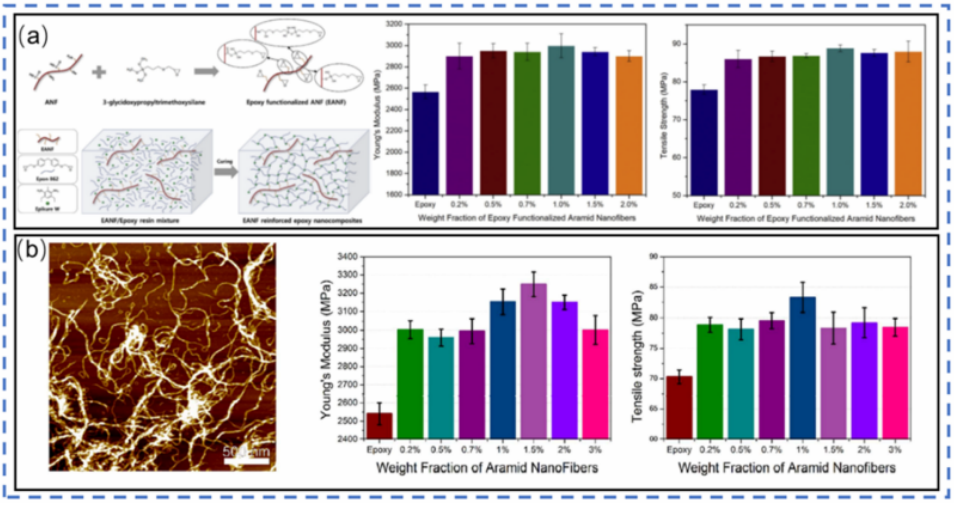

2.5 ANFs reinforced epoxy resin matrix

The use of nanofillers in polymer nanocomposites often improves the overall performance of nanocomposites is improved by boosting stress transfer efficiency between the polymer matrix and fillers (Zhao et al., 2012; Zabihi et al., 2018; Zhang et al., 2020a). Jung and Sodano (2020) the reinforcing effect of the effects of modified ANFs with a glycidyl ether silane coupling agent on the mechanical properties of epoxy resin were investigated. The tensile strength and Young's modulus of nanocomposites EANFs (epoxy-functionalised ANFs) reinforced with 1 wt% epoxy-functionalised ANFs (EANFs) increased by 16.8% and 14.0%, respectively, according to the findings as shown in Figures 6(a) to 6(b). In Lin et al. (2017), a simple and successful method for isolating ANFs, as well as how they were used to build nanocomposites with high elastic modulus and fracture toughness by reinforcing epoxy resin, were also discussed. Iijima and Kamiya (2015) to manufacture functionalised ANFs, silver nanoparticles were uniformly deposited on the surface of ANFs, which were then mixed with epoxy glue to make transparent nanocomposites. In addition, to lower the enhanced adhesive strength and reduce thermal expansion coefficient, m-ANFs reinforced epoxy resin was employed (Oh et al., 2014a, 2014b; On et al., 2017). Furthermore, ANFs have a potential reinforcement impact on a variety of thermoplastic materials thanks to a combination of copolymerisation, layer-by-layer (LBL) assembly, direct blending. To improve the mechanical properties of thermoplastic polyurethane, Koo et al. (2019) created nanoscale ANFs (TPU). That is, TPU toughness has increased 1.5-fold, with a maximum ultimate tensile strength of 84 MPa may be reached with an ANFs concentration of only 0.04% by weight. ANFs provide good reinforcement for epoxy resin matrixes, however non-polar or weakly polar resin matrixes require additional surface modification. As a result, innovative and effective surface modification approaches for ANFs must be investigated.

The benefits of ANF for resin matrix in terms of high impact, dynamic load, temperature resistance and flame.

Even ANFs also blended other matrices like rubber matrix, cellulose, and composite interface. But the better performance of aramid fibre reinforced with epoxy resin matrices gives the good mechanical characteristics for dynamic investigation of composite beam for different volume ratios and boundary conditions.

2.6 Fabrication of composite beam in various processes

Fabrication of FRP composites starts with the manufacture of fibre preforms, which are then reinforced with the matrix material using various procedures. Lacing, braiding, knitting, and sewing fibres together in long mats or sheets produces fibre preforms. With the help of robotics and a high level of automation is utilised to fabricate, allowing on every zone of the moulded item, which has complete control over the angle and content of the fibres (Gascons et al., 2012).

2.6.1 Traditional manufacturing methodologies

Prepregs are made from a blend of fibres and uncured resin that has been pre-impregnated either with the thermoset or thermoplastic resin and just requires thermal activation. These prepregs are materials that are ready to use that are cut and placed down into an open mould (Gascons et al., 2012). They've lost weight in a short amount of time even with coordination with a range of automobile manufacturers, due to the efficient CFRP composite structure fabrication.

The most popular and widely used open mould composite manufacturing process is hand lay-up, as shown in Figure 7. Reinforcements are first placed in a mould and a thin coating of antiadhesive finish is added to make removal easier. The resin component of reinforcing material is poured or applied with a brush. The resin is compressed into the fabrics with the roller, ensuring better contact between the reinforcing layers and the matrix components (Rajak et al., 2019; Sinha et al., 2021).

Figure 7 Process of laying out by hand (see online version for colours)

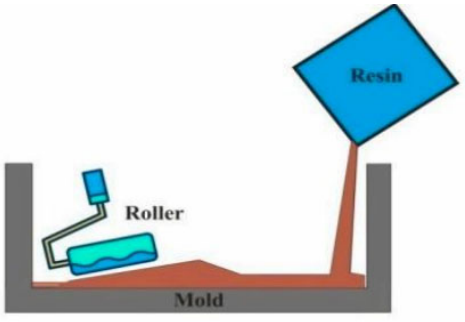

Source: Rajak et al. (2019)

The spray-up technique is the same as the hand-lay-up technique. It, on the other hand, sprays glue and chopped fibres onto a mould with a pistol. At the same time, a roller is utilised to fuse the fibres into the matrix material. Figure 8 depicts the technique.

Chopped fibres are more conformable than hand lay-up in an open mould process and are much faster (Gunge et al., 2019; Perna et al., 2019).

Figure 8 Process of spraying (see online version for colours)

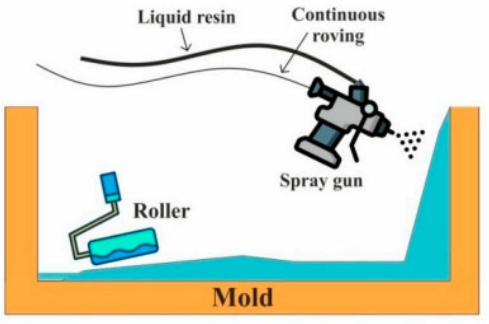

Source: Rajak et al. (2019)

Vacuum bag moulding employs a flexible sheet composed of nylon polyethylene or polyvinyl alcohol to wrap and seal the item from the outside air (PVA). The vacuum bag moulding process is frequently used with the hand lay-up technique. The laminate is made by hand lay-up and sandwiched between the vacuum bag and the moulds to ensure uniform adhere of fibres into the matrix material (Rajak et al., 2019; Fangueiro, 2011; Ervina et al., 2019). The air between the mould and the vacuum bag is removed using a vacuum pump, while the part is compressed using air pressure. Figure 9 depicts the procedure in detail. With gains in interlaminar shear and flexural characteristics of 18% and 15% respectively, using a vacuum bagging procedure, hierarchical composites were created using multiscale carbon fibre reinforcements, which prevented the possibility of observable for dual reinforcements involving porosity and improper impregnation (Tcherdyntsev, 2021).

Figure 9 Vacuum bag moulding process (see online version for colours)

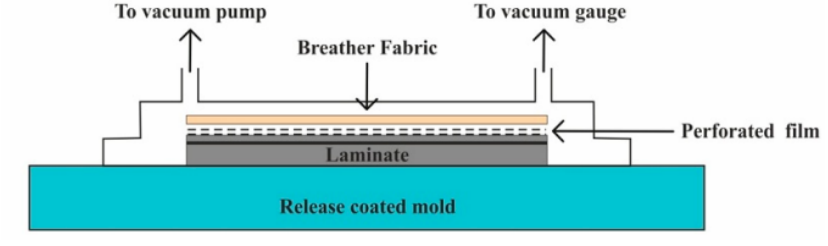

Source: Rajak et al. (2019)

Here injector injects preheated resin under pressure into the composite where reinforcement is in form of a mat or woven roving in the bottom half of the mould (Awan et al., 2018). Figure10 illustrates the mechanics of the RTM stands for resin transfer moulding. RTM supports a wide range of fibre materials and orientations, as well as 3D reinforcements (Jamir et al., 2018; Meola et al., 2016). It produces high-strength, high-quality composite structural pieces whose surface quality equals that of the mould (Nawaz et al., 2018).

Figure 10 Process of resin transfer moulding (see online version for colours)

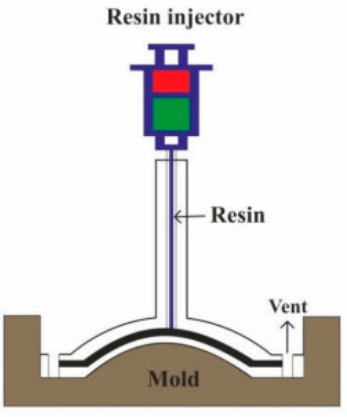

Source: Rajak et al. (2019)

In vacuum infusion or vacuum aided resin transfer moulding, preform fibres are placed on a mould, and a perforated tube is positioned between the vacuum bag and the resin container (VARTM). The resin is pushed using vacuum force via the perforated tubes over the fibres to cement the laminate structure as shown in Figure 11. This approach is used because it removes the presence of air in the composite structure, it is perfect for long structures like boat hulls and wind turbine blades (Davis and Mensah, 2017; Yalcinkaya et al., 2019). Surface treatments are done to natural fibres to improve the strength of woven composites. The tensile strength of an epoxy acrylate resin composite reinforced with alkali-treated flax fibres manufactured utilising the VARTM process increased by 19.7% (Plummer et al., 2011).

Figure 11 Process of vacuum infusion (see online version for colours)

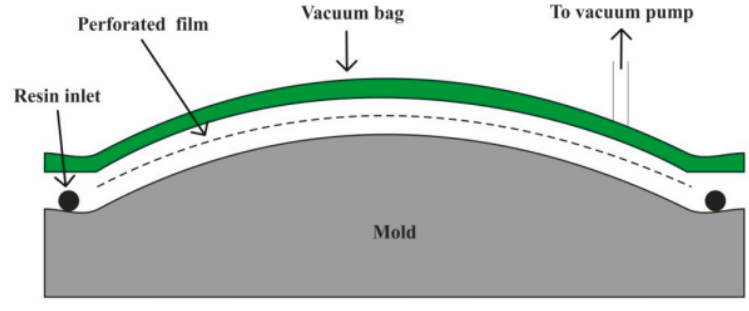

Source: Rajak et al. (2019)

Heat-up mould placed on a mechanical or hydraulic press is used. A ready-to-use reinforcing package made of prepregs is sandwiched between the mould's two sides, which are then pressed together to achieve the required shape. Figure 12 illustrates the compression moulding process in steps. It has a wide range of applications in the automobile industry due to its low cycle time, automation, and high productivity with mechanical properties (Ishikawa et al., 2014). The dispersion of 30% filler elements including sisal fibre was achieved using the compression moulding SEM and Fourier

transform infrared spectrometer analysis revealed that particles of zirconium dioxide (ZrO2) in an unsaturated polyester matrix (UP) had the best mechanical qualities (FTIR), X-ray diffraction (Ciampa et al., 2018). Hand lay-up was used to create an epoxy polymer matrix-based composite with jute fibre reinforcement, which was then compressed at temperatures ranging from 80°C to 130°C. With a determined tensile strength of 32.3 MPa, 41.8 MPa flexural strength, and 3.5 Joules impact strength, the mechanical properties have enhanced (Matveenko et al., 2018).

Figure 12 Compression moulding process (see online version for colours)

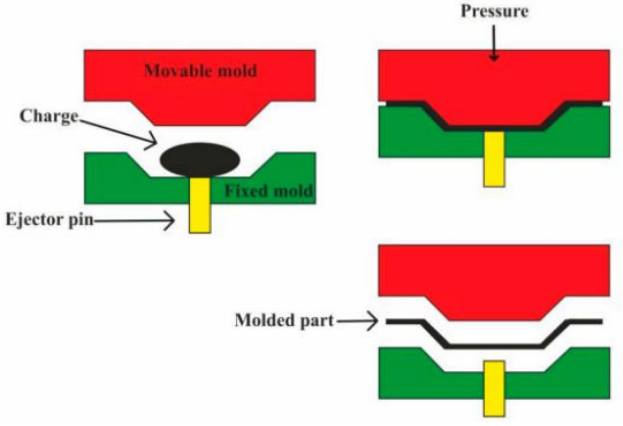

Source: Rajak et al. (2019)

Other than the conventional method of manufacturing the composite even it can be processed along with advanced manufacturing processes like electrospinning process, Injection moulding process (Biswas et al., 2019), and automated manufacturing techniques like automated tape layup (ATL) Filament winding and automated fibre placement (AFP) are used to fabricate the composite of different types of fibre and matrices (Bhardwaj and Kundu, 2010; Mouritz, 2012).

3 Dynamic characterisation of the beam structure

Three-dimensional (3D) bodies like beams consist of one larger dimension than the other two. According to existing circumstances, composite beams and blades have a very advanced theoretical model. Where the dynamic characteristics like vibration analysis of beam can be evaluated by all the approaches that are Experimental, Numerical and Analytical methods to get the results like natural frequencies (ω_n), Damping characteristics (C) and frequency response function (FRF) of the beam.

3.1 Experimental approach

The experimental approach not only includes the analysis of the specimens but also involves the fabrication of composite specimens as discussed above. The focus here is on measuring vibration with the use of a vibration test rig, which is used to perform the free vibration experiment. A support frame, an operation platform, and a vibration exciter

make up the setup rig. The test sample and exciter are suspended from the frame by wire ropes and springs. Clamping, support, and free at the ends of composite beams by using different fixtures setup like clamp-free (C-F), fixed-fixed (F-F), and simply supported beam (S-S) boundary condition (Frketic et al., 2017; Tey et al., 2019).

3.1.1 Experimental setup for vibration analysis

The free vibration experiment is carried out using a vibration test assembly. A support frame, an operation platform, and a vibration exciter are the essential components. Rope wire and springs are used to suspend the test sample and exciter or hammer from the frame. The connections are flexible, and the test sample can appear to be under different conditions. Clamping, support, and free at the end of composite beams by using various fixtures in setup (Tey et al., 2019; Mehar et al., 2017; Zhou et al., 2021). The iron frame was suitably fitted with the test specimens. The fast Fourier transform (FFT) analyser, transducers, laptop, modal hammer, and wires were all connected to the system. The program key for the pulse lab shop version-10.0 will be plugged into the computer's port. For cantilever, free-free, and fixed-fixed boundary conditions, the beams were subjected at a particular location using a minor impact with an impact hammer. A force transducer mounted on the hammer will capture the input signals. An accelerometer was used to detect the associated vibrations of the specimens on the selected location. The signal is sensed by the accelerometer mounted on the specimen with bee's wax, the frequency spectrum is generated when the data is processed by the FFT analyser. A spectrum analyser is used to evaluate both the input and output signals, the derived FRF is then submitted to a computer to extract modal parameters. Using pulse software, the analyser's output will be exhibited on the analyser's screen. Numerous sorts of FRF will be measured directly (Rajak et al., 2019). Here, Figure 13 shows the vibration setup for the beam on the frame with equipment connected in return to the computer for the display of the result (Frketic et al., 2017).

Figure 13 Schematic presentation of experimental vibration setup

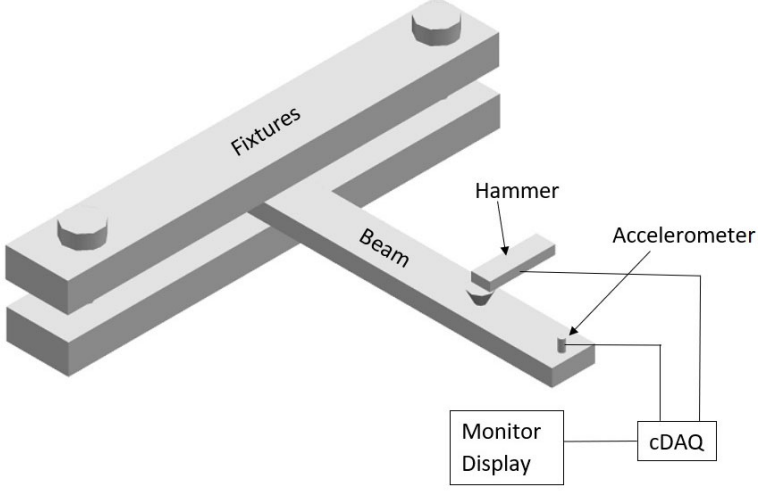

Source: Frketic et al. (2017)

3.1.2 Natural frequencies (ω_n)

As shown by the experimental technique, the effect of delamination on the modal characteristics of a delaminated composite beam is also dependent on the boundary conditions. As the fibre orientation angle increases, the natural frequency of the cantilever boundary condition falls. The natural frequency of a delaminated composite plate increases as the number of layers increases when the cantilever boundary condition is used. As the aspect ratios increase, the delaminated composite cantilever beam's inherent frequency increases (Tita et al., 2003).

The natural frequencies of different composite beam boundary conditions have been published. In general, the experimental results were under the existing literature. Natural frequency is determined to be lowest for clamped-free supported beams and highest for clamped-clamped supported beams (Rafiee et al., 2017).

3.1.3 Damping characteristics (C)

The experimental validation of the current higher-order FE model demonstrates its resilience. When the volume fraction and aspect ratio values grow, the standardised CNRC curved shell panel's fundamental frequency is increasing. The curved shell panel's standard fundamental frequency construction reduces as the thickness and curvature ratio values increase (Frketic et al., 2017).

3.1.4 Frequency response function

Specimens with various fibre orientations and stacking sequences were used in the experimental dynamic tests. Fibre orientations and stacking sequences have an impact on natural frequencies and modal damping was studied. Furthermore, the outcomes of these studies were confirmed by using different software like Labview which encounter all the magnitude of frequency and plot the graph time v/s magnitude for different volume ratio at different boundary conditions.

3.2 Numerical approach

The equations motion of first-order shear deformation theory (FSDT) or Timoshenko beam theory and Hamilton's principle are used to determine the natural frequency and mode shapes. And the effects of boundary conditions on the vibration of ANFs beams are investigated using dynamic models and the effects of ANFs distribution pattern, weight percentage and volume ratio. The accuracy of this new FSDT is comparable to that of the previous FSDT has increased due to adding shear correction factor for convergence of dynamic result. Even dynamic analysis of composite beam also could be found by other various theories like third-order shear deformation theory (TSDT), higher-order shear deformation theory (HSDT), classical lamina beam theory (CLBT) and zeroth-order shear deformation theory (ZSDT) are some examples of refined theories (Mohanty et al., 2012).

3.2.1 Micro-mechanical approach

The effective Young's modulus is evaluated using the modified Halpin-Tsai model, whereas the effective, Poisson's ratio and mass density are computed using the rule of mixture. The FSDT is used to formulate theoretical formulations (Affdl and Kardos, 1976; Thai and Choi, 2013):

1 Longitudinal Young's modulus (E_1):

$$E_1 = V_f E_{1,CN} + V_m E_m \tag{1}$$

2 Transverse Young's modulus (E_2):

$$\frac{E_2}{E_m} = \frac{1+\xi\eta V_f}{1-\eta V_f}$$
$$\eta = \frac{\left(E_f/E_m\right)-1}{\left(E_f/E_m\right)+\xi} \tag{2}$$

ξ is called the reinforcing factor, $\xi = 2$ for a fibre geometry of circular fibres in a square array's packing geometry. Where E_m and E_f are the matrix and reinforcement elastic moduli, respectively. In addition, l denotes the reinforcement's length (Song et al., 2017).

3 In-plane shear modulus (G_{12}):

$$\frac{G_{12}}{G_m} = \frac{1+\xi\eta V_f}{1-\eta V_f}$$
$$\eta = \frac{\left(G_f/G_m\right)-1}{\left(G_f/G_m\right)-\xi}, \qquad \xi = 1 \tag{3}$$

4 Major Poisson's ratio (ϑ_{12}):

$$v_{12} = V_f v_{12,CN} + V_m v_m \tag{4}$$

5 Density (ρ):

$$\rho = V_f \rho_{CN} + V_m \rho_m \tag{5}$$

where V_f and V_m are volume fractions of fibre and matrices, respectively.

3.2.2 Governing equation for FSDT

In terms of thickness co-ordinates, the laminate's displacement functions u, v and w at coordinates x, y, and z are extended in a Taylor series according to the First-Order Shear Deformation theory (Kaw, 2005) where the displacement functions u, v, and w can be expressed as (Zhang et al., 2020b):

$$u = u_0(x, y) + z\theta_x(x, y)$$
$$v = v_0(x, y) + z\theta_y(x, y) \tag{6}$$
$$w = w_0(x, y)$$

Figure 16 Geometry of composite of beam

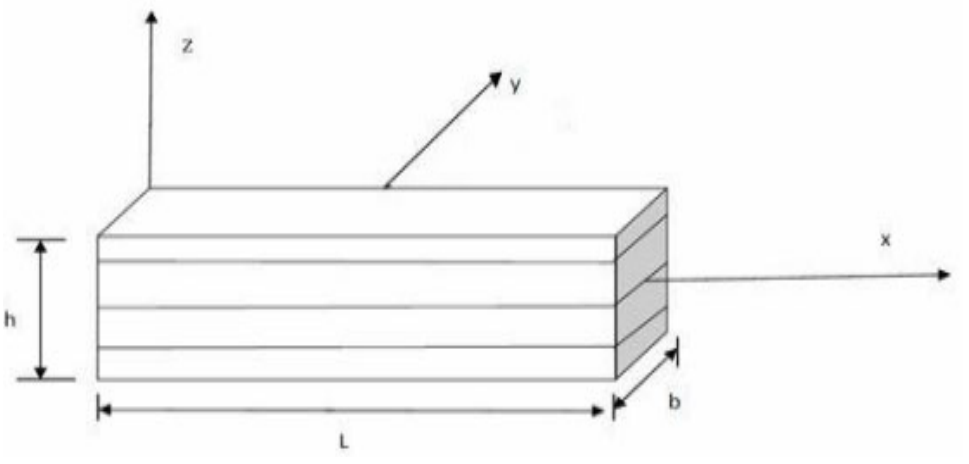

Source: Kaw (2005)

In-plane and transverse displacement components are u, v, and w in the laminate at any point along the x, y, and z-axes. The displacements along the x, y, and z axes are represented by u_0, v_0, and w_0, respectively. θ_x and θ_y are middle plane slopes as well.

3.2.2.1 Elasticity matrix [D]

The beam's strain and displacement relationships are as follows:

$$\begin{aligned}
\varepsilon_x &= \varepsilon_{x_0} + z\kappa_x \\
\varepsilon_y &= \varepsilon_{y_0} + z\kappa_y \\
y_{xy} &= \varepsilon_{xy_0} + z\kappa_{xy} \\
\gamma_{yz} &= \varepsilon_{yz_0} \\
\gamma_{xz} &= \varepsilon_{xz_0}
\end{aligned} \tag{7}$$

Correlation between stress and strain in a beam concerning the fibre matrix coordinate axis (1, 2, and 3) are

$$\begin{Bmatrix} \sigma_1 \\ \sigma_2 \\ \tau_{12} \\ \tau_{23} \\ \tau_{13} \end{Bmatrix} = \begin{bmatrix} C_{11} & C_{12} & 0 & 0 & 0 \\ C_{12} & C_{22} & 0 & 0 & 0 \\ 0 & 0 & C_{44} & 0 & 0 \\ 0 & 0 & 0 & C_{55} & 0 \\ 0 & 0 & 0 & 0 & C_{66} \end{bmatrix} \begin{Bmatrix} \varepsilon_1 \\ \varepsilon_2 \\ \gamma_{12} \\ \gamma_{23} \\ \gamma_{13} \end{Bmatrix} \tag{8}$$

The stresses are (σ_1, σ_2, τ_{12}, τ_{23}, τ_{31}) and the strain components are (ε_1, ε_2, γ_{12}, γ_{23}, γ_{13}) equivalent to the lamina coordinates (1, 2, 3). Appendix A defines C_{ij} as the matrix of compliance about the lamina axis (1, 2, and 3). Laminate coordinates represent the stress-strain relationships for the lamina (x, y, z) as

$$\begin{Bmatrix} \sigma_x \\ \sigma_y \\ \tau_{xy} \\ \tau_{yz} \\ \tau_{xz} \end{Bmatrix} = \begin{bmatrix} Q_{11} & Q_{12} & Q_{14} & 0 & 0 \\ Q_{12} & Q_{22} & Q_{24} & 0 & 0 \\ Q_{14} & Q_{24} & Q_{44} & 0 & 0 \\ 0 & 0 & 0 & KQ_{55} & KQ_{56} \\ 0 & 0 & 0 & KQ_{56} & KQ_{66} \end{bmatrix} \begin{Bmatrix} \varepsilon_x \\ \varepsilon_y \\ \gamma_{xy} \\ \gamma_{yz} \\ \gamma_{xz} \end{Bmatrix} \tag{9}$$

The stresses are (σ_x, σ_y, τ_{xy}, τ_{yz}, τ_{zx}) and the strain components are (ε_x, ε_y, γ_{xy}, γ_{yz}, γ_{zx}) according to the coordinates of the lamination (x, y, z). The modified elasticity constants, known as Q_{ij}'s, are defined in Appendix A.

The factor of shear correction is 0.83 (Shah et al., 2019) is used here. In the consequence of transverse shear stress manifestation, it appears as a coefficient, and it is used to approximate the shear deformation effect. Low shear modulus causes a significant effect on continuous shear deformation in multilayered beam and shell finite elements. The top and bottom sides have zero transverse shear stresses, while the neutral axis has the highest. As both a result of the constant shear distribution over the thickness, accuracy declines. As a result, the shear correction factor must be multiplied by the components of transverse shear stress.

The K's numerical value is calculated by cross-section form, Poisson's ratio, and ply angle for the composite beam. The shear correction factor explains for extension-shear coupling effect. The shear correction factor fits the beam's neutral axis with its axis geometric. The elasticity matrix $[D]$ is obtained as follows:

$$[D] = [T]\left[Q_{ij}\right][T] \tag{10}$$

The thickness coordinate matrix $[T]$ is used here. As a result, the D-matrix for the FSDT can be represented as:

$$[D] = \begin{bmatrix} A_{ij} & B_{ij} & 0 \\ B_{ij} & D_{ij} & 0 \\ 0 & 0 & AA_{ij} \end{bmatrix}$$

$$\left(A_{ij}, B_{ij}, D_{ij}\right) = \int_{-h/2}^{h/2} Q_{ij}\left(1, Z, Z^2\right) dZ \rightarrow i,\ j = 1, 2, 4 \tag{11}$$

$$\left(AA_{ij}\right) = \int_{-h/2}^{h/2} Q_{ij}(1) dZ \rightarrow i,\ j = 5, 6$$

The matrices for extensional stiffness, stretching-bending coupling, and flexural stiffness are $[A_{ij}]$, $[B_{ij}]$, and $[D_{ij}]$ respectively.

3.2.2.2 Strain-displacement matrix

The strain and displacement relation is

$$\{\varepsilon\} = [L]\{\delta\} \tag{12}$$

The operator matrix $[L]$, the in-plane strain matrix, as well as the displacement at any point on the surface element, are all given.

By multiplying the operator matrix by shape functions, the strain-displacement matrix $[B]$ is generated.

$$[B] = [L]^* N_r \rightarrow r = 1, 2, 3, 4, \ldots, 9. \tag{13}$$

As a result, the B-matrix for FSDT can be calculated as follows:

$$[B] = \begin{bmatrix} \frac{\delta N_r}{\delta x} & 0 & 0 & 0 & 0 \\ 0 & \frac{\delta N_r}{\delta y} & 0 & 0 & 0 \\ \delta N_r & \frac{\delta N_r}{\delta x} & 0 & 0 & 0 \\ \frac{\delta y}{0} & 0 & 0 & \frac{\delta N_r}{\delta x} & 0 \\ 0 & 0 & 0 & 0 & \frac{\delta N_r}{\delta y} \\ 0 & 0 & 0 & \frac{\delta N_r}{\delta y} & \frac{\delta N_r}{\delta x} \\ 0 & 0 & \frac{\delta N_r}{\delta y} & 0 & N_r \\ 0 & 0 & \frac{N_r}{\delta x} & & 0 \end{bmatrix} \tag{14}$$

Shape function [*N*]: the interpolation function interpolates the solution between the discrete values collected at each element's mesh nodes.

$$\begin{aligned} N_i &= 1/4\left(\xi^2 + \xi_i\xi\right)\left(\eta^2 + \eta_i\eta\right); \rightarrow i = 1, 2, 3, 4 \\ N_i &= 1/2\left(1-\xi^2\right)\left(\eta^2 + \eta_i\eta\right); \rightarrow i = 5, 7 \\ N_i &= 1/2\left(\xi^2 + \xi_i\xi\right)\left(1-\eta^2\right); \rightarrow i = 6, 8 \\ N_i &= \left(1-\xi^2\right)\left(1-\eta^2\right); \rightarrow i = 9. \end{aligned} \tag{15}$$

The issuing domain is in the physical coordinate system, whereas the natural coordinate system is in the natural coordinate system. (ζ, η, ξ) is used (x, y, and z).

3.2.2.3 Mass matrix [M]

The composite beam element's element mass matrix is

$$[M_e] = \int_{(A_c)} [N]'[\rho][N]dA \tag{16}$$

where [ρ] matrix for FSDT is

$$[\rho]=\begin{bmatrix} I & 0 & P & 0 & 0 \\ 0 & I & 0 & 0 & P \\ 0 & 0 & I & 0 & 0 \\ P & 0 & 0 & Q & 0 \\ 0 & P & 0 & 0 & Q \end{bmatrix} \tag{17}$$

3.2.2.4 Element stiffness matrix [K]

The matrix of element stiffness for the considered beam element is

$$[K_e]=\int_{A_c}[B]'[D][B]dA \tag{18}$$

The following free vibration equation is generated by combining all of them about the global coordinate's matrix of element mass and stiffness. Non-dimensional natural frequency of beam by using Bernoulli-Euler theory $\omega_n=\frac{(1.8751)^2}{2\pi L^2}\sqrt{\frac{EI}{\rho_L}}$ (Song et al., 2018).

$$[K]-\omega_n^2[M]=0 \tag{19}$$

In the Gauss quadrature method, the stiffness [*K*] and mass [*M*] matrices are integrated using this method. The above formula gives the natural frequency (ω_n) for free vibration (Park, 2015). Appendix B explains the methodology used in the analysis.

3.2.3 Methodology for FEM

Bellifa et al. (2016) compared the classic First-order and other higher-order shear deformation theories were used to explain the bending and free vibration analysis of functionally graded beams, while a simple shear deformation theory with the fewest unknowns was used to explain the bending and free vibration analysis of functionally graded beams.

Nguyen et al. (2013) FSDT was used to express axially loaded functionally graded beams: static and free vibration.

Shahba et al. (2011) the finite element method was used to examine free vibration and stability of axially functionally graded Timoshenko tapered beams utilising classical and neoclassical boundary conditions.

Hosseini-Hashemi et al. (2010) presented to solve exact equations of motion, and analytical analysis based on the FSDT is used. The mechanical properties of the FG plates were anticipated to change constantly with thickness throughout the study. There's also a new shear correction factor formula. The influence of various base stiffness parameters, as well as different values of aspect ratios and gradient indices, on the free vibration of FG plates restricted by various combinations of classical boundary conditions, was then discussed.

Figure 17 Flowchart for finding natural frequency by FSDT (see online version for colours)

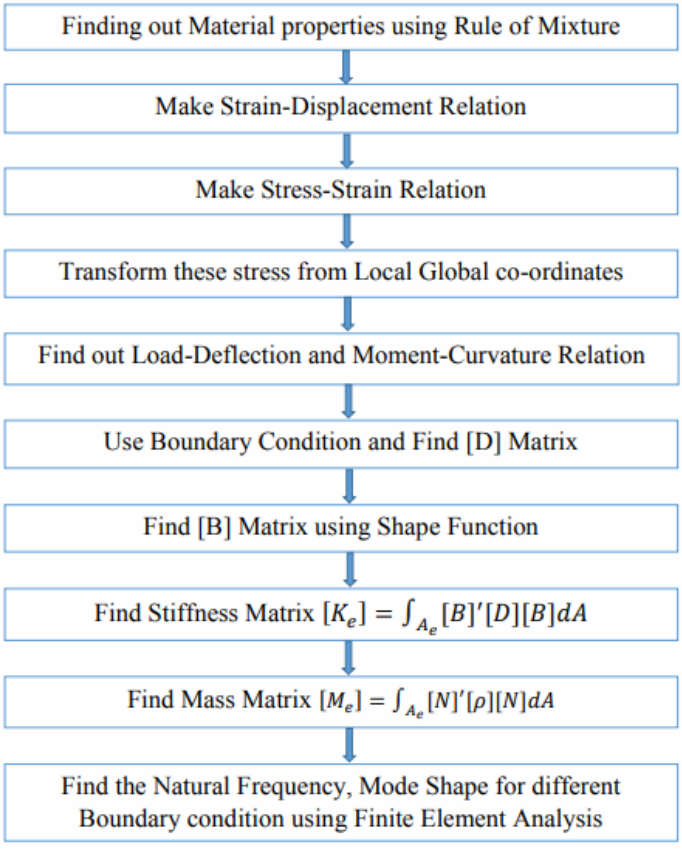

Bahmyari et al. (2014) carried out the dynamic response of LCB under distributed moving masses utilising Based on both FSDT and classical beam theory, the finite element method (FEM) was developed (CLT). CLT and FSDT equations of motion are used to discretise beam elements with six and ten degrees of freedom, respectively. As a result, the beam governing equations, which include the Coriolis, effects using Newmark's technique, inertial and centrifugal forces due to moving distributed mass were spatially discretised and analysed in the time domain. The effect of moving body speed, incline angle, mass, load length, inertial, Coriolis, layer orientation, and centrifugal forces by moving distributed mass, as well as friction force, on the dynamic characteristics of inclined LCB was investigated.

Ganesh et al. (2016), using the equivalent single layer (ESL) theory and the finite element method, explored the free vibration analysis of delaminated composite plates (FEM). Their study focuses solely on the free vibration analysis of delaminated composite plates utilising the FSDT and FE formulation. Simply supported (S-S-S-S) and cantilever type boundary conditions were used in the study (C-F-F-F). In addition to that using a fully analytical and computational technique, the deformation of the composite plate at various locations was evaluated.

Table 2 Results and discussion of different composite beam and their dynamic behaviour on the various boundary condition

Sl. no.	*Type of composite*	*Boundary condition*	*Analytical ω_n (Hz)*	*Numerical ω_n (Hz)*	*Experimental ω_n (Hz)*	*Critical finding*	*Ref*
1	FG beam of Al/ZrO_2	S-S C-S S-F	37.276 39.483 33.710	-	-	Here, the analytical calculation of ω_n increases as the aspect ratio and volume ratio of fibre increases	Hosseini-Hashemi et al. (2010)
2	Composite beam of graphite/epoxy	C-C C-S	3.865 2.960	-	-	The ω_n for both types of support, conditions diminish as the angle of orientation increases from 0 to 90 degrees, according to this study.	Krishnaswamy et al. (1992)
3	Spinning composite beam boron-epoxy composite material	C-F	13.72	14.500	-	For the spinning composite shaft with cantilever end conditions, the first three natural frequencies and mode forms are shown.	Banerjee and Su (2006, 2004)
4	sisal and banana natural fibres Hybrid composite beam	C-F	-	-	507	Chemical treatment raises the modulus of the material and rigidity of the composite, affecting natural frequencies indirectly.	Rajesh et al. (2016)
5	Carbon/epoxy composite beam	C-C C-F S-S	-	120.9 61.7 88.82	-	In the clamped-free boundary condition, the slope of the nonlinear vibration curve was higher and lower than the linear vibration curve at the clamped and free ends, respectively.	Ghasemi et al. (2016)
6	FG-CNT reinforced composite beams	C-C C-H H-H C-F	-	6.0025 5.8204 5.6247 4.0915	-	The frequency of laminated FG-CNTRC beams is substantially influenced by boundary conditions, CNT volume fractions, and length-to-thickness ratios.	Vo-Duy et al. (2019)
7	Glass-polyester composite beam	C-C C-S F-F C-F S-S	-	2,614.3 2,576.0 2,619.4 1,490.4 2,567.9	-	For all boundary conditions, it can be seen that the classical theory over-predicts the natural frequencies. Shear deformation, in other words, has the effect of lowering natural frequencies.	Jun et al. (2008)

Table 2 Results and discussion of different composite beam and their dynamic behaviour on the various boundary condition (continued)

Sl. no.	*Type of composite*	*Boundary condition*	*Analytical* ω_n *(Hz)*	*Numerical* ω_n *(Hz)*	*Experimental* ω_n *(Hz)*	*Critical finding*	*Ref*
8	Woven-glass-polyester LCB	S-S	23.42	24.140	-	Natural frequency reduces as delamination length increases. As the ply angle changes from 0 to 90, the natural frequency falls.	Çallioğlu and Atlihan (2011)
9	Aloe vera and glass reinforcement epoxy composite beam	C-C	-	4,770.9	4,695.8	The natural frequency of Aloe Vera reinforced glass-epoxy is the lowest. With increasing modes of analysis, the natural frequency tends to have a positive slope in all circumstances.	Thomas et al. (2018)
		C-F		3,122.4	3,098.6		
		C-S		4,770.7	4,684.6		
10	E-glass woven roving fibres and polyester matrix composite beam	C-F	-	121.7	121.0	The experimental study, which used specifically prepared beam specimens with varying fibre volume ratios, turned out to be reasonable.	Aly et al. (2010)
11	Graphite/epoxy composite beam	C-F	-	621.25	633.23	For a variety of ply layups, natural frequencies and mode shapes were shown.	Hodges et al. (1991) and Minguet and Dugundji (1990)
12	Laminated carbon/epoxy composite beam	C-C		2,661.9	2,546.2	Dynamic behaviour of laminated composite beams, which will be used as an experimental benchmark in the frequency domain.	Das and Sahu (2021)
		F-F		5,610.4	5,578.1		
13	Graphite epoxy delaminated composites	F-F		109.04	109.03	The impact of composite geometry, as well as the locations, sizes, and amount of delamination, on composite vibration characteristics, are examined parametrically.	Lee (2000)
14	CNT/Al-alloy composite beams with functional grades	S-S	2.971	2.8500	-	It was discovered that when the values of VCNT increased, the amplitudes of displacements decreased.	Civalek et al. (2021) and Arvin et al. (2010)

Table 2 Results and discussion of different composite beam and their dynamic behaviour on the various boundary condition (continued)

Sl. no.	*Type of composite*	*Boundary condition*	*Analytical* ω_n *(Hz)*	*Numerical* ω_n *(Hz)*	*Experimental* ω_n *(Hz)*	*Critical finding*	*Ref*
15	Carbon/epoxy LCB	C-F	-	256.4	-	The C-C boundary condition has the maximum natural frequencies, whereas the S-S boundary condition has the least. The C-F boundary conditions have natural frequencies which are slightly more than the S-S condition	Rajeshkumar and Hariharan (2012)
		S-S		201.4			
		C-C		1,104.5			
16	Glass/epoxy composite plates	SSSS	-	349.4	330.0	For the cantilever boundary condition, the natural frequency of a delaminated composite plate grows as the number of layers increases.	Tita et al. (2003)
		CCCC		471.2	450.0		
		CFFF		128.4	135.7		
17	Glass fibre composite beam	C-F	-	361.4	360	Without adding bulk or modifying geometry, you may achieve the necessary natural frequencies and damping factors.	Mehar et al. (2017)
18	Glass fibre sandwich composite beam with a viscoelastic layer	C-F	-	2,276.5	-	Only soft cores showed a decrease in natural frequencies, whereas hard cores showed an increase in natural frequencies.	Taber and Viano (1982)
19	Taper glass and aluminium fibre LCB	C-F	-	2,769.91	2,684.24	For a wide range of engineering applications, the uniform beam element gives a suitably accurate solution.	Taber and Viano (1982)
20	F glass – polyester composite beam	C-C	-	5,794.2	-	For all boundary circumstances, the natural frequency of all modes is found to be extremely sensitive to a smaller layup angle than a higher layup angle. The poison effect cannot be overlooked because it has a significant impact on all modes.	Talekar and Kotambkar (2020)
		C-S		5,653.6			
		C-F		4,359.6			
		S-S		5,496.0			
		F-F		6,754.6			

Table 2 Results and discussion of different composite beam and their dynamic behaviour on the various boundary condition (continued)

Sl. no.	*Type of composite*	*Boundary condition*	*Analytical* ω_n *(Hz)*	*Numerical* ω_n *(Hz)*	*Experimental* ω_n *(Hz)*	*Critical finding*	*Ref*
21	Graphite-epoxy LCB	C-C	487.63	-	-	The influence of inclination angle on beam indicates that as the inclination angle increases, the natural frequencies increase.	Bahmyari et al. (2014)
22	S-glass-epoxy LCB	SS	2.848	2.8491	-	In a beam with a C-C boundary condition, the maximum, minimum natural frequency, and deflection were found.	Kahya (2012)
		CC	6.450	6.4586			
		CS	-	4.4509			
		CF	1.015	1.0150			
23	W-graphite-epoxy	CC	4.8487	4.8629	-	The inherent frequency of a graphite-epoxy composite beam is around 2.5 times that of a standard steel beam.	Kadivar and Mohebpour (1998)
24	Graphite-epoxy beams	SS	30·8386	30·0061	-	In both approaches, the maximum natural frequency is found in the CC border condition.	[Shi and Lam (1999)
		CC	31·2874	31·2144			
		CS	31·0569	30·6107			
		CF	26·2118	25·9931			
23	FGM alumina (Al_2O_3) with SE-glass fibre	SS	11.1640	11.0739	-	In both approaches, the FGM Beam's natural frequency is validated.	Şimşek and Kocatürk (2009)
24	FG-CNTRC beam	C-C	-	126.489	124.28	It was discovered that as the volume ratio rises, the natural frequency rises as well.	Heshmati and Yas (2013)
25	E-glass/epoxy LCB	CC	-	761.8	765.79	It was discovered that as the volume fibre ratio varies, the frequency changes as well, and the increase in radio frequency follows suit.	Sinha et al. (2021)
		SS		234.2	220.44		
		CF		492.29	493.99		
26	FG MWCNT composite	CF	-	61.9613	63.9985	It was discovered that when the ply angle increases, so does the natural frequency.	Uymaz (2013)

Table 2 Results and discussion of different composite beam and their dynamic behaviour on the various boundary condition (continued)

Sl. no.	*Type of composite*	*Boundary condition*	*Analytical* ω_n *(Hz)*	*Numerical* ω_n *(Hz)*	*Experimental* ω_n *(Hz)*	*Critical finding*	*Ref*
27	Functionally graded CNT beams	SC	-	55.589	56.150	The frequency of all beams increases as the aspect ratio of the beam increases. Cantilever beams have a more severe increase in CP.	Lin and Yang (2014)
		CP		72.258	73.068		
28	FGM beams of CNTRC	HH	-	224.51	224.55	The nonlinear frequency ratios of both H–H and C–H FG-CNTRC beams are affected by the sign of the vibration amplitudes since their nonlinear frequency ratio vs. amplitude graphs are not balanced.	Ke et al. (2010)
		CC		139.83	139.87		
		CH		169.58	167.20		
29	FGM ceramic and MWCNT	CF	3,865.4	3,723.1	-	For dynamic characteristics, the FGM is tested both with and without the FGM beam.	Chakraborty et al. (2003)
30	FG E-glass and SWCNT	CC	828.49	828.30	-	The effects of the aspect ratio and various material compositions on the FG Nano beam's static and stability responses are described here.	Şimşek and Yurtcu (2013)
31	Graphite/epoxy LCB	CF	579	546	-	For natural frequency, the results are confirmed using the FEM method.	Koo and Lee (1995)
32	SE-glass-polymer matrices composite	CF	27.03	-	27.04	The natural frequency lowers as the volume of fibre decreases.	Huang and Su (2008)
		PP	75.79		75.81		
		FP	118.38		118.52		
		FF	171.79		171.93		
33	Carbon/epoxy lamina composite	FF	-	6,390	5,949.85	When LCB is compared to Cast Iron Bar, it is found that LCB with geometry has a higher natural frequency than Cast Iron.	Aly et al. (2010)

Table 2 Results and discussion of different composite beam and their dynamic behaviour on the various boundary condition (continued)

Sl. no.	*Type of composite*	*Boundary condition*	*Analytical* ω_n *(Hz)*	*Numerical* ω_n *(Hz)*	*Experimental* ω_n *(Hz)*	*Critical finding*	*Ref*
34	Carbon fibre-reinforced polymer (CFRP) composites beam	CC	-	582.5	659.42	Based on the multiple parameters tested, the best dynamic properties of the composite plate were also identified using an optimisation technique.	Gopalan et al. (2021)
		FF		1,001.25	1,096.23		
35	Carbon fibres polymer composite beam	CF	-	560.23	597.65	The natural frequency of the beam increases as the number of carbon fibres in the beam increases.	Dhakal and Sain (2020)
34	Graphite-epoxy material LCB	CS	-	4,950.7	4,712.5	It is evident that as the axial force increases, the frequency lowers, and the decline accelerates as the axial force approaches buckling stress.	Li et al. (2008)
		FF		4,971.4	4,951.1		
		CF		3,120.7	3,089.8		
		SS		4,949.4	4,949.0		
35	Graphite/epoxy beam LCB	CF	98.1380	93.0608	-	Natural frequencies are affected by the number of plies, height/width ratios, slenderness ratios, material types, and boundary conditions.	Yildirim et al. (1999)
		CS	145.462	135.296			
		CC	153.278	141.082			
36	D-graphite/epoxy beam	SS	11.9145	10.534	-	The frequency increases as the number of layers in composite increases for both cross-ply and angle-ply beams, but the percentage increase and then decreases.	Chandrashekhara and Bangera (1992)
		CC	14.1999	16.574			
		CS	13.0579	11.9506			
		CF	9.2162	10.7609			
37	R-glass/epoxy LCB	CF	-	99.95	87.51	When the volume of fibre rises, the frequency is gradually adjusted.	Karthik et al. (2021)
38		SS	215.24	220.24	-	The first three vibration modes and natural frequencies are explored in connection to material attributes.	Giunta et al. (2013)

Table 2 Results and discussion of different composite beam and their dynamic behaviour on the various boundary condition (continued)

Sl. no.	*Type of composite*	*Boundary condition*	*Analytical* ω_n *(Hz)*	*Numerical* ω_n *(Hz)*	*Experimental* ω_n *(Hz)*	*Critical finding*	*Ref*
39	D-graphite-epoxy symmetric cross-ply beams	FF	16.210	16.211	-	As the L/h ratio drops, the frequencies suggested by the various assumptions increase. In all of the cases below, FSDBT forecasts the highest frequencies.	Aydogdu (2005)
		CC	15.685	15.682			
		SF	11.224	11.225			
		CS	11.059	11.058			
		SS	7.218	7.218			
		CF	2.590	2.590			
40	W-graphite-epoxy composite beam	CC	-	15.2920	15.0981	A combination of the state space approach and the differential quadrature method was used to examine the natural frequencies of laminated beams. Their method is based on CLBT and takes a variety of boundary conditions into account.	Gunda et al. (2011) and Chen et al. (2004)
		SS		13.2745	11.9145		
		CF		9.3750	9.2162		
41	E-glass fibre with hard core epoxy resin LCB	CC	2824	2,781.882	-	Natural frequencies are investigated about the core-to-face thickness ratio and the flexible core shear modulus.	Della and Shu (2005)
		CF	184.0243	172.8510			
		SS	184.0243	162.8256			
42	MWCN/epoxy LCB	CC	-	287.34	312.5	For different thickness ratios of the curved beam, five alternative geometries, and two types of boundary conditions, the fundamental frequencies of the CNRC curved panel were determined.	Chen et al. (2003)
		SS		118.48	119.8		
43	Polypropylene fibres and ethylene matrices	CF	56.953	-	57.542	The experimental data and the finite element model were found to be closely linked.	Hu et al. (2002)
		SS	80.740		79.750		

Table 2 Results and discussion of different composite beam and their dynamic behaviour on the various boundary condition (continued)

Sl. no.	*Type of composite*	*Boundary condition*	*Analytical* ω_n *(Hz)*	*Numerical* ω_n *(Hz)*	*Experimental* ω_n *(Hz)*	*Critical finding*	*Ref*
44	Metal fibre and epoxy matrices	CF	-	238.10	246.60	The natural frequency drops when the volume ratio of metal fibre in composite lowers.	Banerjee et al. (2008)
45	CFRP LCB	SS	-	578.1	602.5	Because the use of a continuous model necessitates a suitable effective area, the difference in natural frequencies between the present methodology and the finite element method is less than 9% under the condition that the ratio of hole and plate areas is less than 7%.	Kim and Park (2020)
		CC		998.7	1,023.7		
46	Single-ply glass-epoxy composite	FF		1,292.62	1,288.35	The two - dimensional map-based approach can easily spot and locate damage, according to the numerical and experimental results.	Manoach et al. (2017)
47	MWCNT composite beam	CF	-	152.18	152.32	MWCNTs can also be made more compatible with the Polymer matrix by using different production procedures or chemical modifications.	Rokni et al. (2012)
48	Carbon-epoxy	SS	2,052.4955	2,067.2430	-	By increasing the number of elements, good convergence and accuracy of the first three frequencies parameters can be achieved.	Kheladi et al. (2021)
49	Isotropic and symmetrically laminated composite beams	SS	896.42	-	-	The SS boundary condition has a higher natural frequency than the CF.	Doeva et al, (2021)
		CF	672.97				

Table 2 Results and discussion of different composite beam and their dynamic behaviour on the various boundary condition (continued)

Sl. no.	*Type of composite*	*Boundary condition*	*Analytical* ω_n *(Hz)*	*Numerical* ω_n *(Hz)*	*Experimental* ω_n *(Hz)*	*Critical finding*	*Ref*
50	Glass-polyester beam	CC	5,167.5	-	-	Raising the extensional modulus E1 increases the natural frequencies of the beam, which has a substantial impact on higher frequencies.	Jun et al. (2009)
		CS	5,166.6				
		FF	5,270.1				
		CF	3,323.2				
		SS	5,166.3				
51	FRP of D-glass fibre composite beam	CF	687.4	702.4	-	With a specific fibre volume ratio and the same fibre material, the greatest influence on variation in stiffness and natural frequencies is attained.	Tilahun and Lemu (2020)
52	E-glass fibre-reinforced composite beam	CF	-	315.4	335.19	In several boundary conditions, including cantilever, simply supported, fixed-simply supported, and fixed-ended situations, the first three natural frequencies of composite beams are examined and analysed. The method can be repeated for composite beams with varied layer orientations and volume percentages.	Kumar and Rao (2017)
		FS		780.7	801.2		
		SS		540.6	610.476		
		CC		943.1	998.64		
53	Glass fibre-reinforced polymer and graphene filler	FF	-	1,098.4	1,201.8	When the weight proportion of graphene utilised in composite beams is reduced, the bending natural frequencies improve dramatically.	Pawgi et al. (2021)
		CF		760.2	802.3		
54	E-glass/epoxy resin LCB	CF	-	-	19.508	As the fibre orientation angle grows from 0 to 80, the fundamental frequency behaviour diminishes.	Torabi et al. (2016)

Table 2 Results and discussion of different composite beam and their dynamic behaviour on the various boundary condition (continued)

Sl. no.	*Type of composite*	*Boundary condition*	*Analytical* ω_n *(Hz)*	*Numerical* ω_n *(Hz)*	*Experimental* ω_n *(Hz)*	*Critical finding*	*Ref*
55	Glass/carbon hybrid composite beams	CF	-	-	766	The beam's increased flexural strength and stiffness produce modified deformation characteristics in free vibration.	Evran (2020)
56	GFRP composite beams	CC	1,076.641	1,074.32	1,104.5	As the volume of fibre grows, the frequency of specimens increases as well.	Gemi et al. (2021)
57	Carbon/epoxy composite beams	CF	-	576.9	610.5	As the carbon volume in the beam grows, the composite's toughness increases, and the natural frequency improves.	Das and Sahu (2021)
		CC		1,001.63	1,044.7		
58	Carbon nanotubes (CNTs) polymer matrix LCB	SS	6.951	6.716	-	The frequencies of CNTRC beams drop like the fact that change in waviness in fibre distribution is increased.	Heshmati et al. (2015)
59	Functionally graded graphene platelets LCB	CC	-	79.688	79.726	The frequency-amplitude relationship for deeply curved beams is significantly nonlinear.	Polit et al. (2019)
		CP		64.635	59.925		
		PP		48.996	42.864		
60	FG-CNT reinforced composite beams	CF	0.1831	0.2054		As the rotational speed increases, the natural frequencies of the CC, CS, and SS beams decrease, and the natural frequency also decreases as the temperature rises.	Xu et al. (2021)
		CC	0.8947	0.7319			
		SS	0.3370	0.4238			

Balci et al. (2014) conducted a simulation study based on Euler-Bernoulli or classical beam theory, free vibration analysis of an LCB is conducted. And also using the finite element approach, a numerical model of the LCB was developed for various boundary conditions based on varying (l/h) ratios for many layers by FSDT. The LCB's natural frequencies were determined for each boundary condition and shown in such a way that the influence of these modifications on the natural frequencies could be seen. For varying (L_x/h) ratios, layer angles, several layers, and their respective placements, eight natural frequencies for boundary conditions such as clamped-clamped (CC), simple-simple (SS), and clamped-free (C-F) composite beams were first produced. In all cases, natural frequencies for all modes decreased as the l/h ratio grew.

Wang et al. (2019) examined fundamental frequencies for graphene oxide powders-reinforced composite beams that were used in the vibration study (GPORC). The fundamental frequency of the C-C beam is higher than the beam with the H-H boundary condition, according to the comparison. It's also worth noting that as the slenderness ratio rises, the fundamental frequency falls. The greatest fundamental frequency is found in the X-GOPRC beam, which is the U-GPORC and O-GPORC beams are then followed.

4 Conclusions

An extensive literature review has been conducted on the fabrication and analysis of dynamic characteristics as composite beams via numerical and experimental approaches with different boundary conditions. Based on the resources available the following conclusions are drawn:

- The different reinforcement and matrices materials are used to manufacture the composite beam structure. Most of the researchers used the compression moulding technique to fabricate composite.
- The natural frequency is mainly dependent on fibre orientation, aspect ratio and type of boundary conditions.
- The volume fraction ratio of fibre and matrices, the number of reinforcing layers, and the thickness of the matrices affect the damping behaviour of beam structures.
- Increasing the number of fibre layers or volume can improve the material's strength, dynamic behaviour and stiffness, allowing it to undergo free vibration without putting a high load on it and reducing the material's tendency to crack or break.

References

Affdl, J.H. and Kardos, J.L. (1976) 'The Halpin-Tsai equations: a review', *Polymer Engineering & Science*, Vol. 16, No. 5, pp.344–352.

Aly, M.F., Goda, I.G.M. and Hassan, G.A. (2010) 'Experimental investigation of the dynamic characteristics of laminated composite beams', *International Journal of Mechanical and Mechatronics*, Vol. 10, No. 3, pp.59–68.

Arvin, H., Sadighi, M. and Ohadi, A.R. (2010) 'A numerical study of free and forced vibration of composite sandwich beam with viscoelastic core', *Composite Structures*, Vol. 92, No. 4, pp.996–1008.

Awan, F.S., Fakhar, M.A., Khan, L.A., Zaheer, U., Khan, A.F. and Subhani, T. (2018) 'Interfacial mechanical properties of carbon nanotube-deposited carbon fiber epoxy matrix hierarchical composites', *Composite Interfaces*, Vol. 25, No. 8, pp.681–699.

Aydogdu, M. (2005) 'Vibration analysis of cross-ply laminated beams with general boundary conditions by Ritz method', *International Journal of Mechanical Sciences*, Vol. 47, No. 11, pp.1740–1755.

Bahmyari, E., Mohebpour, S.R. and Malekzadeh, P. (2014) 'Vibration analysis of inclined laminated composite beams under moving distributed masses', *Shock and Vibration*, Vol. 2014, Article no. 750916.

Balci, M., Nalbant, M.O., Kara, E. and Gündogdu, Ö. (2014) 'Free vibration analysis of a laminated composite beam with various boundary conditions', *International Journal of Automotive and Mechanical Engineering*, Vol. 9, No. 1746, p.1734.

Banerjee, J.R. and Su, H. (2004) 'Development of a dynamic stiffness matrix for free vibration analysis of spinning beams', *Computers & Structures*, Vol. 82, Nos. 23–26, pp.2189–2197.

Banerjee, J.R. and Su, H. (2006) 'Dynamic stiffness formulation and free vibration analysis of a spinning composite beam', *Computers & Structures*, Vol. 84, Nos. 19–20, pp.1208–1214.

Banerjee, J.R., Su, H. and Jayatunga, C. (2008) 'A dynamic stiffness element for free vibration analysis of composite beams and its application to aircraft wings', *Computers & Structures*, Vol. 86, No. 6, pp.573–579.

Bellifa, H., et al. (2016) 'Bending and free vibration analysis of functionally graded plates using a simple shear deformation theory and the concept the neutral surface position', *Journal of the Brazilian Society of Mechanical Sciences and Engineering*, Vol. 38, No. 1, pp.265–275.

Bhardwaj, N. and Kundu, S.C. (2010) 'Electrospinning: a fascinating fiber fabrication technique', *Biotechnology Advances*, Vol. 28, No. 3, pp.pp–325-347.

Biswas, B., Hazra, B., Sarkar, A., Bandyopadhyay, N.R., Mitra, B.C. and Sinha, A. (2019) 'Influence of ZrO2 incorporation on sisal fiber reinforced unsaturated polyester composites', *Polymer Composites*, Vol. 40, No. 7, pp.2790–2801.

Çallioğlu, H. and Atlihan, G. (2011) 'Vibration analysis of delaminated composite beams using analytical and FEM models', Vol. 18, pp.7–14.

Cao, K., Siepermann, C.P., Yang, M., Waas, A.M., Kotov, N.A., Thouless, M.D. and Arruda, E.M. (2013) 'Reactive aramid nanostructures as high-performance polymeric building blocks for advanced composites', *Advanced Functional Materials*, Vol. 23, No. 16, pp.2072–2080.

Chakraborty, A., Gopalakrishnan, S. and Reddy, J.N. (2003) 'A new beam finite element for the analysis of functionally graded materials', *International Journal of Mechanical Sciences*, Vol. 45, No. 3, pp.519–539.

Chandrashekhara, K. and Bangera, K.M. (1992) 'Free vibration of composite beams using a refined shear flexible beam element', *Computers & Structures*, Vol. 43, No. 4, pp.719–727.

Chen, W.Q., Lv, C.F. and Bian, Z.G. (2003) 'Elasticity solution for free vibration of laminated beams', *Composite Structures*, Vol. 62, No. 1, pp.75–82.

Chen, W.Q., Lv, C.F. and Bian, Z.G. (2004) 'Free vibration analysis of generally laminated beams via state-space-based differential quadrature', *Composite Structures*, Vol. 63, Nos. 3–4, pp.417–425.

Cheng, M., Chen, W. and Weerasooriya, T. (2005) 'Mechanical properties of Kevlar® KM2 single fiber', *J. Eng. Mater. Technol.*, Vol. 127, No. 2, pp.197–203.

Ciampa, F., Mahmoodi, P., Pinto, F. and Meo, M. (2018) 'Recent advances in active infrared thermography for non-destructive testing of aerospace components', *Sensors*, Vol. 18, No. 2, p.609.

Civalek, Ö. et al. (2021) 'Forced vibration analysis of composite beams reinforced by carbon nanotubes', *Nanomaterials*, Vol. 11, No. 3, p.571.

Das, P. and Sahu, S.K. (2021) 'Free vibration analysis of industry-driven woven fiber laminated carbon/epoxy composite beams by experimental and numerical approach', *Polymers and Polymer Composites*, Vol. 29, No. 9_suppl, pp.S1371–S1385.

Davis, D.C. and Mensah, T.O. (2017) 'Fabrication and fatigue of fiber-reinforced polymer nanocomposites – a tool for quality control', in Mensah, T.O., Wang, B., Bothun, G., Winter, J. and Davis, V. (Eds.): *Nanotechnology Commercialization: Manufacturing Processes and Products*, American Institute of Chemical Engineering, John Wiley and Sons Inc.

Deitzel, J.M., Kleinmeyer, J., Harris, D.E.A. and Tan, N.B. (2001) 'The effect of processing variables on the morphology of electrospun nanofibers and textiles', *Polymer*, Vol. 42, No. 1, pp.261–272.

Della, C.N. and Shu, D. (2005) 'Free vibration analysis of composite beams with overlapping delaminations', *European Journal of Mechanics-A/Solids*, Vol. 24, No. 3, pp.491–503.

Dhakal, H.N. and Sain, M. (2020) 'Enhancement of mechanical properties of flax-epoxy composite with carbon fibre hybridisation for lightweight applications', *Materials*, Vol. 13, No. 1, p.109.

Doeva, O., Masjedi, P.K. and Weaver, P.M. (2021) 'A semi-analytical approach based on the variational iteration method for static analysis of composite beams', *Composite Structures*, Vol. 257, p.113110.

Erdelyi, N.H. and Hashemi, S.M. (2016) 'On the finite element free vibration analysis of delaminated layered beams: a new assembly technique', *Shock and Vibration*, Vol. 2016, No. 3707658, p.1155.

Ervina, J., Ghaleb, Z.A., Hamdan, S. and Mariatti, M. (2019) 'Colloidal stability of water-based carbon nanotube suspensions in electrophoretic deposition process: Effect of applied voltage and deposition time', *Composites Part A: Applied Science and Manufacturing*, Vol. 117, No. 1016, pp.1–10.

Evran, S. (2020) 'Experimental and statistical free vibration analyses of laminated composite beams with functionally graded fiber orientation angles', *Polymers and Polymer Composites*, Vol. 28, No. 7, pp.513–520.

Fan, J., Shi, Z., Zhang, L., Wang, J. and Yin, J. (2012) 'Aramid nanofiber-functionalized graphene nanosheets for polymer reinforcement', *Nanoscale*, Vol. 4, No. 22, pp.7046–7055.

Fangueiro, R. (Ed.) (2011) *Fibrous and Composite Materials for Civil Engineering Applications*, Woodhead Publishing, Elsevier.

Frketic, J., Dickens, T. and Ramakrishnan, S. (2017) 'Automated manufacturing and processing of fiber-reinforced polymer (FRP) composites: an additive review of contemporary and modern techniques for advanced materials manufacturing', *Additive Manufacturing*, Vol. 14, No. 3, pp.69–86.

Ganesh, S., Kumar, K.S. and Mahato, P.K, (2016) 'Free vibration analysis of delaminated composite plates using finite element method', *Procedia Engineering*, Vol. 144, No. 2, pp.1067–1075.

Gascons, M., Blanco, N. and Matthys, K. (2012) 'Evolution of manufacturing processes for fiber-reinforced thermoset tanks, vessels, and silos: a review', *IIE Transactions*, Vol. 44, No. 6, pp.pp–476-489.

Gemi, L., Madenci, E. and Özkılıç, Y.O. (2021) 'Experimental, analytical and numerical investigation of pultruded GFRP composite beams infilled with hybrid FRP reinforced concrete', *Engineering Structures*, Vol. 244, p.112790.

Ghasemi, A.R. et al. (2016) 'Nonlinear free vibration of an Euler-Bernoulli composite beam undergoing finite strain subjected to different boundary conditions', *Journal of Vibration and Control*, Vol. 22, No. 3, pp.799–811.

Giunta, G. et al. (2013) 'Free vibration analysis of composite beams via refined theories', *Composites Part B: Engineering*, Vol. 44, No. 1, pp.540–552.

Gonzalez, G.M., MacQueen, L.A., Lind, J.U., Fitzgibbons, S.A., Chantre, C.O., Huggler, I., Golecki, H.M., Goss, J.A. and Parker, K.K. (2017) 'Production of synthetic, para-aramid and biopolymer nanofibers by immersion rotary jet-spinning', *Macromolecular Materials and Engineering*, Vol. 302, No. 1, p.1600365.

Gopalan, V. et al. (2021) 'Dynamic characteristics of woven flax/epoxy laminated composite plate', *Polymers*, Vol. 13, No. 2, p.209.

Grujicic, M., Yavari, R., Ramaswami, S., Snipes, J.S., Yen, C.F. and Cheeseman, B.A. (2013) 'Molecular-level study of the effect of prior axial compression/torsion on the axial-tensile strength of PPTA fibers', *Journal of Materials Engineering and Performance*, Vol. 22, No. 11, pp.3269–3287.

Gunda, J.B. et al. (2011) 'Large amplitude vibration analysis of composite beams: simple closed-form solutions', *Composite Structures*, Vol. 93, No. 2, pp.870–879.

Gunge, A., Koppad, P.G., Nagamadhu, M., Kivade, S.B. and Murthy, K.S. (2019) 'Study on mechanical properties of alkali treated plain woven banana fabric reinforced biodegradable composites', *Composites Communications*, Vol. 13, No. 10, pp.47–51.

Heshmati, M. and Yas, M.H. (2013) 'Free vibration analysis of functionally graded CNT-reinforced nanocomposites beam using Eshelby-Mori-Tanaka approach', *Journal of Mechanical Science and Technology*, Vol. 27, No. 11, pp.3403–3408.

Hodges, D.H. et al. (1991) 'Free-vibration analysis of composite beams', *Journal of the American Helicopter Society*, Vol. 36, No. 3, pp.36–47.

Hosseini-Hashemi, S., Taher, H.R.D., Akhavan, H. and Omidi, M. (2010) 'Free vibration of functionally graded rectangular plates using first-order shear deformation plate theory', *Applied Mathematical Modelling*, Vol. 34, No. 5, pp.1276–1291.

Hu, N. et al. (2002) 'Vibration analysis of delaminated composite beams and plates using a higher-order finite element', *International Journal of Mechanical Sciences*, Vol. 44, No. 7, pp.1479–1503.

Huang, C.W. and Su, Y.H. (2008) 'Dynamic characteristics of partial composite beams', *International Journal of Structural Stability and Dynamics*, Vol. 8, No. 4, pp.665–685.

Huang, Y., Wang, D., Xu, L., Cong, Y., Li, J. and Li, L. (2013) 'Multiscale fibers via supramolecular self-assembly of a fully rigid, discotic aromatic aramid molecule', *European Polymer Journal*, Vol. 49, No. 6, pp.1682–1687.

Huang, Z.M., Zhang, Y.Z., Ramakrishna, S. and Lim, C.T. (2004) 'Electrospinning and mechanical characterization of gelatin nanofibers', *Polymer*, Vol. 45, No. 15, pp.5361–5368.

Ifuku, S., Maeta, H., Izawa, H., Morimoto, M. and Saimoto, H. (2014) 'Facile preparation of aramid nanofibers from Twaron fibers by a downsizing process', *RSC Advances*, Vol. 4, No. 76, pp.40377–40380.

Iijima, M. and Kamiya, H. (2015) 'Non-aqueous colloidal processing route for fabrication of highly dispersed aramid nanofibers attached with Ag nanoparticles and their stability in epoxy matrixes', *Colloids and Surfaces A: Physicochemical and Engineering Aspects*, Vol. 482, pp.195–202.

Inman, D.J. and Singh, R.C. (1994) *Engineering Vibration*, Vol. 3, Prentice Hall, Englewood Cliffs, NJ.

Ishak, M.R., Sapuan, S.M., Leman, Z., Rahman, M.Z.A., Anwar, U.M.K. and Siregar, J.P. (2013) 'Sugar palm (Arenga pinnata): its fibres, polymers and composites', *Carbohydrate polymers*, Vol. 91, No. 2, pp.699–710.

Ishikawa, H. et al. (2014) 'Effect of surface treatments on the mechanical properties of natural fiber textile composites made by VaRTM method', *Composite Interfaces*, Vol. 21, No. 4, pp.329–336.

Jamir, M.R., Majid, M.S. and Khasri, A. (2018) 'Natural lightweight hybrid composites for aircraft structural applications', *Sustainable Composites for Aerospace Applications*, pp.155–170, Woodhead Publishing, Elsevier.

Jun, L., Hongxing, H. and Rongying, S. (2008) 'Dynamic finite element method for generally laminated composite beams', *International Journal of Mechanical Sciences*, Vol. 50, No. 3, pp.466–480.

Jun, Li, Li, X. and Hua, H. (2009) 'Free vibration analysis of third-order shear deformable composite beams using dynamic stiffness method', *Archive of Applied Mechanics*, Vol. 79, No. 12, pp.1083–1098.

Jung, J. and Sodano, H.A. (2020) 'High strength epoxy nanocomposites reinforced by epoxy functionalized aramid nanofibers', *Polymer*, Vol. 195, p.122438.

Kadivar, M.H. and Mohebpour, S.R. (1998) 'Finite element dynamic analysis of unsymmetric composite laminated beams with shear effect and rotary inertia under the action of moving loads', *Finite elements in Analysis and Design*, Vol. 29, Nos. 3–4, pp.259–273.

Kahya, V. (2012) 'Dynamic analysis of laminated composite beams under moving loads using finite element method', *Nuclear Engineering and Design*, Vol. 243, pp.41–48.

Karthik, R. et al. (2021) 'Numerical analysis of vibration characteristics and mechanical properties of polyoxymethylene/cloisite polymer nanocomposites', *Materials Today: Proceedings*, Vol. 45, pp.874–878.

Kaw, A.K. (2005) *Mechanics of Composite Materials*, CRC Press, Taylor and Francis publication.

Ke, L-L., Yang, J. and Kitipornchai, S. (2010) 'Nonlinear free vibration of functionally graded carbon nanotube-reinforced composite beams', *Composite Structures*, Vol. 92, No. 3, pp.676–683.

Dupont (2019) *Kevlar Aramid Fiber Technical Guide* [online] https://www.dupont.com/ (accessed April 2019).

Kheladi, Z., Hamza-Cherif, S.M. and Ghernaout, M.E.A. (2021) 'Free vibration analysis of variable stiffness laminated composite beams', *Mechanics of Advanced Materials and Structures*, Vol. 28, No. 18, pp.1889–1916.

Kim, Y. and Park, J. (2020) 'A theory for the free vibration of a laminated composite rectangular plate with holes in aerospace applications', *Composite Structures*, Vol. 251, No. 1, p.112571.

Koo, J.M., Kim, H., Lee, M., Park, S.A., Jeon, H., Shin, S.H., Kim, S.M., Cha, H.G., Jegal, J., Kim, B.S. and Choi, B.G. (2019) 'Nonstop monomer-to-aramid nanofiber synthesis with remarkable reinforcement ability', *Macromolecules*, Vol. 52, No. 3, pp.923–934.

Koo, K-N. and Lee, I. (1995) 'Dynamic behavior of thick composite beams', *Journal of Reinforced Plastics and Composites*, Vol. 14, No. 3, pp.196–210.

Krishnaswamy, S., Chandrashekhara, K. and Wu, W.Z.B. (1992) 'Analytical solutions to vibration of generally layered composite beams', *Journal of Sound and Vibration*, Vol. 159, No. 1, pp.85–99.

Kulkarni, A., Bambole, V.A. and Mahanwar, P.A. (2010) 'Electrospinning of polymers, their modeling and applications', *Polymer – Plastics Technology and Engineering*, Vol. 49, No. 5, pp.427–441.

Kumar, C.S. and Rao, D.S. (2017) 'Numerical and experimental vibration analysis of laminated composite beam at different boundary conditions', Vol. 7, No. 4, pp.38–44.

Lee, J. (2000) 'Free vibration analysis of delaminated composite beams', *Computers & Structures*, Vol. 74, No. 2, pp.121–129.

Li, J., Hua, H. and Shen, R. (2008) 'Dynamic stiffness analysis for free vibrations of axially loaded laminated composite beams', *Composite Structures*, Vol. 84, No. 1, pp.87–98.

Lin, F. and Yang, X. (2014) 'Vibration of carbon nanotube reinforced composite beams based on the first and third order beam theories', *Applied Mathematical Modelling*, Vol. 38, Nos. 15–16, pp.3741–3754.

Lin, J., Bang, S.H., Malakooti, M.H. and Sodano, H.A. (2017) 'Isolation of aramid nanofibers for high strength and toughness polymer nanocomposites', *ACS Applied Materials & Interfaces*, Vol. 9, No. 12, pp.11167–11175.

Luo, J., Zhang, M., Yang, B., Liu, G. and Song, S. (2019) 'Fabrication and characterization of differentiated aramid nanofibers and transparent films', *Applied Nanoscience*, Vol. 9, No. 5, pp.631–645.

Manoach, E. et al. (2017) 'Numerical and experimental studies on vibration based methods for detection of damage in composite beams', *Composite Structures*, Vol. 170, pp.26–39.

Matveenko, V.P., Kosheleva, N.A., Shardakov, I.N. and Voronkov, A.A. (2018) 'Temperature and strain registration by fibre-optic strain sensor in the polymer composite materials manufacturing', *International Journal of Smart and Nano Materials*, Vol. 9, No. 2, pp.99–110.

Mehar, K., Panda, S.K. and Mahapatra, T.R. (2017) 'Theoretical and experimental investigation of vibration characteristic of carbon nanotube reinforced polymer composite structure', *International Journal of Mechanical Sciences*, Vol. 133, pp.319–329.

Meola, C., Boccardi, S. and Carlomagno, G.M. (Eds.) (2016) *Infrared Thermography in the Evaluation of Aerospace Composite Materials: Infrared Thermography to Composites*. Woodhead Publishing, Elsevier.

Minguet, P. and Dugundji, L. (1990) 'Experiments and analysis far composite blades under large deflections. Part II – dynamic behavior', *AIAA Journal*, September, Vol. 28, No. 9.

Mohanty, J., Sahu, S.K. and Parhi, P.K. (2012) 'Numerical and experimental study on free vibration of delaminated woven fiber glass/epoxy composite plates', *International Journal of Structural Stability and Dynamics*, Vol. 12, No. 2, pp.377–394.

Mouritz, A.P. (2012) *Introduction to Aerospace Materials*, Woodhead Publishing, Elsevier.

Nasser, J., Lin, J., Steinke, K. and Sodano, H.A. (2019) 'Enhanced interfacial strength of aramid fiber reinforced composites through adsorbed aramid nanofiber coatings', *Composites Science and Technology*, Vol. 174, No. 12, pp.125–133.

Nawaz, A., Islam, B., Khattak, M.S., Ali, L., Saleem, U., Ullah, A., Ijaz, M.Z. and Mao, W. (2018) 'Polyester usage in manufacturing of electrical and mechanical products and assemblies', *Polyester-Production, Characterization and Innovative Applications*, IntechOpen.

Nguyen, T.K., Vo, T.P. and Thai, H.T. (2013) 'Static and free vibration of axially loaded functionally graded beams based on the first-order shear deformation theory', *Composites Part B: Engineering*, Vol. 55, pp.147–157.

Nirmala, R., Navamathavan, R., Park, S.J. and Kim, H.Y. (2014) 'Recent progress on the fabrication of ultrafine polyamide-6 based nanofibers via electrospinning: a topical review', *Nano-Micro Letters*, Vol. 6, No. 2, pp.89–107.

Oh, H.J., Han, S.H., Kim, H.Y. and Kim, S.S. (2014a) 'The influence of the core–shell structured meta-aramid/epoxy nanofiber mats on interfacial bonding strength and the mechanical properties of epoxy adhesives at cryogenic environment', *Journal of Adhesion Science and Technology*, Vol. 28, No. 10, pp.950–962.

Oh, H.J., Kim, H.Y. and Kim, S.S. (2014b) 'Effect of the core/shell-structured meta-aramid/epoxy nanofiber on the mechanical and thermal properties in epoxy adhesive composites by electrospinning', *The Journal of Adhesion*, Vol. 90, No. 9, pp.787–801.

On, S.Y., Kim, M.S. and Kim, S.S. (2017) 'Effects of post-treatment of meta-aramid nanofiber mats on the adhesion strength of epoxy adhesive joints', *Composite Structures*, Vol. 159, pp.636–645.

Park, C.H. (2015) 'Numerical simulation of flow processes in composites manufacturing', *Advances in Composites Manufacturing and Process Design*, pp.317–378, Woodhead Publishing, Elsevier.

Park, S., Park, K., Yoon, H., Son, J., Min, T. and Kim, G. (2007) 'Apparatus for preparing electrospun nanofibers: designing an electrospinning process for nanofiber fabrication', *Polymer International*, Vol. 56, No. 11, pp.1361–1366.

Pawgi, A. et al. (2021) 'Influence of graphene fillers on vibration characteristics of tapered hybrid GFRP composite beams under elevated temperature condition: Numerical and experimental study', *Journal of Vibration and Control*, p.10775463211045795.

Perna, A.S., Viscusi, A., Astarita, A., Boccarusso, L., Carrino, L., Durante, M. and Sansone, R. (2019) 'Manufacturing of a metal matrix composite coating on a polymer matrix composite through cold gas dynamic spray technique', *Journal of Materials Engineering and Performance*, Vol. 28, No. 6, pp.3211–3219.

Pham, Q.P., Sharma, U. and Mikos, A.G. (2006) 'Electrospinning of polymeric nanofibers for tissue engineering applications: a review', *Tissue Engineering*, Vol. 12, No. 5, pp.1197–1211.

Plummer, C.J.G., Bourban, P.E. and Månson, J.A. (2011) 'Polymer matrix composites: matrices and processing', *Encyclopedia of Materials: Science and Technology*, pp.7388–7396, Elsevier.

Polit, O., B. Pradyumna, and M. Ganapathi. (2019) 'Large amplitude free flexural vibrations of functionally graded graphene platelets reinforced porous composite curved beams using finite element based on trigonometric shear deformation theory', *International Journal of Non-Linear Mechanics*, Vol. 116, No. 6, pp.302–317.

Teijin (2019) *Product Brochure: Twaron*, [online] https://www.teijinaramid.com/en/products/twaron/ (accessed December 2019).

Rafiee, M., Nitzsche, F. and Labrosse, M. (2017) 'Dynamics, vibration and control of rotating composite beams and blades: a critical review', *Thin-Walled Structures*, Vol. 119, pp.795–819.

Rajak, D.K., Pagar, D.D., Menezes, P.L. and Linul, E. (2019) 'Fiber-reinforced polymer composites: Manufacturing, properties, and applications', *Polymers*, Vol. 11, No. 10, p.1667.

Rajesh, M., Pitchaimani, J. and Rajini, N.J.P.E. (2016) 'Free vibration characteristics of banana/sisal natural fibers reinforced hybrid polymer composite beam', *Procedia Engineering*, Vol. 144, No. 10, pp.1055–1059.

Rajeshkumar, G. and Hariharan, V. (2012) 'Free vibration analysis of hybrid-composite beams', *IEEE – International Conference on Advances in Engineering, Science and Management (ICAESM-2012)*, IEEE.

Rao, Y., Waddon, A.J. and Farris, R.J. (2001) 'Structure-property relation in poly (p-phenylene terephthalamide) (PPTA) fibers', *Polymer*, Vol. 42, No. 13, pp.5937–5946.

Rapakousiou, A., López-Moreno, A., Nieto-Ortega, B., Bernal, M.M., Monclús, M.A., Casado, S., Navío, C., González, L.R., Fernández-Blázquez, J.P., Vilatela, J.J. and Pérez, E.M. (2020) 'Stronger aramids through molecular design and nanoprocessing', *Polymer Chemistry*, Vol. 11, No. 8, pp.1489–1495.

Roenbeck, M.R., Cline, J., Wu, V., Afshari, M., Kellner, S., Martin, P., Londono, J.D., Clinger, L.E., Reichert, D., Lustig, S.R. and Strawhecker, K.E. (2019) 'Structure-property relationships of aramid fibers via X-ray scattering and atomic force microscopy', *Journal of Materials Science*, Vol. 54, No. 8, pp.6668–6683.

Rokni, H. et al. (2012) 'Improvement in dynamic properties of laminated MWCNT-polystyrene composite beams via an integrated numerical-experimental approach', *Composite Structures*, Vol. 94, No. 8, pp.2538–2547.

Shah, S.A., Sharma, E.M. and Sharma, P. (2019) 'Vibration analysis of composite beam', *International Journal for Technological Research in Engineering*, Vol. 6, No. 12, pp.2347–4718.

Shahba, A., Attarnejad, R., Marvi, M.T. and Hajilar, S. (2011) 'Free vibration and stability analysis of axially functionally graded tapered Timoshenko beams with classical and non-classical boundary conditions', *Composites Part B: Engineering*, Vol. 42, No. 4, pp.801–808.

Shi, G. and Lam, K.Y. (1999) 'Finite element vibration analysis of composite beams based on higher-order beam theory', *Journal of Sound and Vibration*, Vol. 219, No. 4, pp.707–721.

Şimşek, M. and Kocatürk, T. (2009) 'Free and forced vibration of a functionally graded beam subjected to a concentrated moving harmonic load', *Composite Structures*, Vol. 90, No. 4, pp.465–473.

Şimşek, M. and Yurtcu, H.H. (2013) 'Analytical solutions for bending and buckling of functionally graded nanobeams based on the nonlocal Timoshenko beam theory', *Composite Structures*, Vol. 97, No. 38, pp.378–386.

Sinha, L. et al. (2021) 'Experimental and numerical study on free vibration characteristics of laminated composite plate with/without cut-out', *Composite Structures*, Vol. 256, p.113051.

Sinha, L., Das, D., Nayak, A.N. and Sahu, S.K. (2021) 'Experimental and numerical study on free vibration characteristics of laminated composite plate with/without cut-out', *Composite Structures*, Vol. 256, p.113051.

Song, M., Kitipornchai, S. and Yang, J. (2017) 'Free and forced vibrations of functionally graded polymer composite plates reinforced with graphene nanoplatelets', *Composite Structures*, Vol. 159, No. 1, pp.579–588.

Song, M., Yang, J. and Kitipornchai, S. (2018) 'Bending and buckling analyses of functionally graded polymer composite plates reinforced with graphene nanoplatelets', *Composites Part B: Engineering*, Vol. 134, pp.106–113.

Taber, L.A. and Viano, D.C. (1982) 'Comparison of analytical and experimental results for free vibration of non-uniform composite beams', *Journal of Sound and Vibration*, Vol. 83, No. 2, pp.219–228.

Talekar, N. and Kotambkar, M. (2020) 'Free vibration analysis of generally layered composite beam with various lay-up and boundary conditions', *Materials Today: Proceedings*, Vol. 21, pp.1283–1292.

Tcherdyntsev, V.V. (2021) 'Reinforced Polymer Composites', *Polymers*, Vol. 13, No. 4, p.564.

Tey, J., Soon, Y.Y., Cheo, T., Ooi, K.H., Ho, F., Vellayappan, B., Chia, D. and Tai, B.C. (2019) 'Efficacy of palliative bladder radiotherapy for hematuria in advanced bladder cancer using contemporary radiotherapy techniques', *In Vivo*, Vol. 33, No. 6, pp.2161–2167.

Thai, H.T. and Choi, D.H. (2013) 'A simple first-order shear deformation theory for laminated composite plates', *Composite Structures*, Vol. 106, No. 6, pp.754–763.

Thomas, P., Jenarthanan, M.P. and Sreehari, V.M. (2018) 'Free vibration analysis of a composite reinforced with natural fibers employing finite element and experimental techniques', *Journal of Natural Fibers*, Vol. 17, No. 5, pp.688–699.

Tilahun, N.D. and Lemu, H.G. (2020) 'Mechanical vibration analysis of fiber reinforced polymer composite beams using analytical and numerical methods', *International Conference on Advances of Science and Technology*, Springer, Cham,.

Tita, V., de Carvalho, J. and Lirani, J. (2003) 'Theoretical and experimental dynamic analysis of fiber reinforced composite beams', *Journal of the Brazilian Society of Mechanical Sciences and Engineering*, Vol. 25, No. 3, pp.306–310.

Torabi, K., Shariati-Nia, M. and Heidari-Rarani, M. (2016) 'Experimental and theoretical investigation on transverse vibration of delaminated cross-ply composite beams', *International Journal of Mechanical Sciences*, Vol. 115, No. 116, pp.1–11.

Uymaz, B. (2013) 'Forced vibration analysis of functionally graded beams using nonlocal elasticity', *Composite Structures*, Vol. 105, No. 227, pp.227–239.

Vo-Duy, T., Ho-Huu, V. and Nguyen-Thoi, T. (2019) 'Free vibration analysis of laminated FG-CNT reinforced composite beams using finite element method', *Frontiers of Structural and Civil Engineering*, Vol. 13, No. 2, pp.324–336.

Wang, Y., Xie, K., Fu, T. and Shi, C. (2019) 'Bending and elastic vibration of a novel functionally graded polymer nanocomposite beam reinforced by graphene nanoplatelets', *Nanomaterials*, Vol. 9, No. 12, p.1690.

Wu, Y., Wang, F. and Huang, Y. (2019) 'Facile fabrication and performance comparison of aramid-nanofiber membrane formed by water or ethanol', *Polymer Composites*, Vol. 40, No. 6, pp.2534–2538.

Xu, J. et al. (2021) 'Free vibration analysis of rotating FG-CNT reinforced composite beams in thermal environments with general boundary conditions', *Aerospace Science and Technology*, Vol. 118, p.107030.

Yalcinkaya, M.A. et al. (2019) 'Pressurized infusion: a new and improved liquid composite molding process', *Journal of Manufacturing Science and Engineering*, Vol. 141, No. 1, p.12.

Yan, H., Li, J., Tian, W., He, L., Tuo, X. and Qiu, T. (2016) 'A new approach to the preparation of poly (p-phenylene terephthalamide) nanofibers', *RSC Advances*, Vol. 6, No. 32, pp.26599–26605.

Yang, B., Wang, L., Zhang, M., Luo, J. and Ding, X. (2019a) 'Timesaving, high-efficiency approaches to fabricate aramid nanofibers', *ACS Nano*, Vol. 13, No. 7, pp.7886–7897.

Yang, B., Wang, L., Zhang, M., Luo, J., Lu, Z. and Ding, X. (2020) 'Fabrication, applications, and prospects of aramid nanofiber', *Advanced Functional Materials*, Vol. 30, No. 22, p.2000186.

Yang, B., Zhang, M. and Lu, Z. (2017) 'Effects of potassium titanate whiskers on the mechanical and thermal properties of poly (para-phenylene terephthalamide) paper sheet', *Polymer Composites*, Vol. 38, No. 7, pp.1390–1395.

Yang, M. et al. (2011) 'Dispersions of aramid nanofibers: a new nanoscale building block', *ACS nano*, Vol. 5, No. 9, pp.6945–6954.

Yang, M., Cao, K., Yeom, B., Thouless, M.D., Waas, A., Arruda, E.M. and Kotov, N.A. (2015) 'Aramid nanofiber-reinforced transparent nanocomposites', *Journal of Composite Materials*, Vol. 49, No. 15, pp.1873–1879.

Yang, X., Guo, Y., Han, Y., Li, Y., Ma, T., Chen, M., Kong, J., Zhu, J. and Gu, J. (2019b) 'Significant improvement of thermal conductivities for BNNS/PVA composite films via electrospinning followed by hot-pressing technology', *Composites Part B: Engineering*, Vol. 175, No. 16, p.107070.

Yao, J., Jin, J., Lepore, E., Pugno, N.M., Bastiaansen, C.W. and Peijs, T. (2015) 'Electrospinning of p-aramid fibers', *Macromolecular Materials and Engineering*, Vol. 300, No. 12, pp.1238–1245.

Yao, L., Lee, C. and Kim, J. (2010) 'Fabrication of electrospun meta-aramid nanofibers in different solvent systems', *Fibers and Polymers*, Vol. 11, No. 7, pp.1032–1040.

Yildirim, V., Sancaktar, E. and Kiral, E. (1999) 'Free vibration analysis of symmetric cross-ply laminated composite beams with the help of the transfer matrix approach', *Communications in Numerical Methods in Engineering*, Vol. 15, No. 9, pp.651–660.

Yoshioka, Y. (2012) 'Fabrication and characterization of fluorine-containing aromatic polyamide nanofiber mats', *e-Journal of Surface Science and Nanotechnology*, Vol. 10, pp.74–78.

Yoshioka, Y. (2017) 'Structural changes of aromatic polyamide nanofibers upon annealing treatment', *International Journal of Polymer Analysis and Characterization*, Vol. 22, No. 2, pp.169–179.

Yoshioka, Y. and Tashiro, K. (2014) 'Self-assembled aromatic polyamide nanofibers with trifluoromethyl groups via precipitation polymerization', *Colloids and Surfaces A: Physicochemical and Engineering Aspects*, Vol. 447, pp.148–154.

Zabihi, O., Ahmadi, M., Nikafshar, S., Preyeswary, K.C. and Naebe, M. (2018) 'A technical review on epoxy-clay nanocomposites: Structure, properties, and their applications in fiber reinforced composites', *Composites Part B: Engineering*, Vol. 135, No. 15, pp.1–24.

Zhang, B., Wang, W., Tian, M., Ning, N. and Zhang, L. (2020a) 'Preparation of aramid nanofiber and its application in polymer reinforcement: a review', *European Polymer Journal*, Vol. 139, p.109996.

Zhang, Z., Li, Y., Wu, H., Zhang, H., Wu, H., Jiang, S. and Chai, G. (2020b) 'Mechanical analysis of functionally graded graphene oxide-reinforced composite beams based on the first-order shear deformation theory', *Mechanics of Advanced Materials and Structures*, Vol. 27, No. 1, pp.3–11.

Zhao, S., Song, Z., Cui, J., Li, C. and Yan, Y. (2012) 'Improving dispersion and integration of single-walled carbon nanotubes in epoxy composites by using a reactive noncovalent dispersant', *Journal of Polymer Science Part A: Polymer Chemistry*, Vol. 50, No. 21, pp.4548–4556.

Zhou, Z., Chen, M., Xiong, Y., Jia, W., Dong, W. and Xie, K. (2021) 'Experimental and mixed analytical–numerical studies for free and forced vibrations of Z-reinforced sandwich plates stiffened by steel ribs', *Composite Structures*, Vol. 272, p.114221.

Appendix A

When $m = \cos\theta$ and $n = \sin\theta$. The transformed [Q] matrix coefficient are:

$$Q_{11} = C_{11}m^4 + 2\left(C_{12} + 2C_{44}\right)m^2n^2 + C_{22}n^4,$$

$$Q_{12} = C_{12}\left(m^4 + n^4\right) + \left(C_{11} + C_{22} - 4C_{44}\right)m^2n^2,$$

$$Q_{13} = C_{13^{m^2}} + C_{23^{n^2}},$$

$$Q_{14} = \left(C_{11} - C_{22} - 2C_{44}\right)m^3n + \left(C_{11} - C_{22} + 2C_{44}\right)mn^3,$$

$$Q_{22} = C_{11^4}^4 + \left(2\left(C_{12} + 4C_{44}\right)^{m^2n^2 + C_{22^m}}\right)^4$$

$$Q_{23} = C_{13^n}^2 + \left(C_{23}^m\right)^2,$$

$$Q_{24} = \left(C_{11} - C_{22} - 2C_{44}\right)mn^3 + \left(C_{11} - C_{22} + 2C_{44}\right)m^3n,$$

$$Q_{33} = C_{33},$$

$$Q_{34} = \left(c_{31} - c_{32}\right)mn,$$

$$Q_{44} = \left(C_{11} - 2C_{12} + C_{22} - 2C_{44}\right)m^2n^2 + C_{44}\left(m^4 + n^4\right)$$

$$Q_{55} = C_{55^m}^2 + C_{66^n}^2$$

$$Q_{66} = C_{55^N}^2 + C_{66}m^2$$

And compliance matrix coefficient are:

$$C_{22} = \frac{E_2\left(1 - v_{13}v_{31}\right)}{\Delta}, \quad C_{23} = \frac{E_2\left(v_{32} + v_{12}v_{31}\right)}{\Delta}, \quad C_{33} = \frac{E_3\left(1 - v_{12}v_{21}\right)}{\Delta},$$

$$C_{44} = G_{12}, \quad C_{55} = G_{23}, \quad C_{66} = G_{13}.$$

Appendix B

Gauss-Quadrature method

The Gauss-Legendre quadrature is highly beneficial for polynomial function integration. It can use the n points exactly to integrate a polynomial function of order ($2n$ – 1). If we take a finite number of calculations in numerical integration. As a result, the integral is estimated to be:

$$\int_a^b f(x)dx = \sum_{i=1}^{M} f\left(x_i\right)W_i$$

where

M number of points of integration

X_i point of integration or sampling

W_i coefficient of weight.

The width of a rectangular strip with a height of $f(x_i)$ can be regarded as the weighing coefficient. This form can be used to express any numerical integration. The integration domain is standardised to $-1 \leq x \leq -1$ in order to generate standard values for the integration points and weighting coefficient.

As a result, the stiffness and mass matrices are mixed in the following way:

$$[K_e] = \int_{-1}^{1}\int_{-1}^{1} [B]'[D][B]|J|\, d\xi d\eta$$

$$[M_e] = \int_{-1}^{1}\int_{-1}^{1} [N]'[\rho][N]|J|\, d\xi d\eta$$

The Jacobian matrix $|J|$ has the following definition:

$$[J] = \begin{bmatrix} \frac{dx}{d\xi} & \frac{dy}{d\xi} \\ \frac{dx}{d\eta} & \frac{dy}{d\eta} \end{bmatrix}$$

Here, generalised coordinates x and y are used, while natural coordinates ξ and η are used.